A Wireless Optical Backhaul Solution for Optical Attocell Networks

A Wireless Optical Backhaul Solution
for Optical Attocell Networks

Hossein Kazemi, *Student Member, IEEE,* Majid Safari, *Member, IEEE,* and Harald Haas, *Fellow, IEEE*

Abstract—The problem of backhauling for optical attocell networks has been approached by a number of wired solutions such as in-building power line communication (PLC), Ethernet and optical fiber. In this paper, an alternative solution is proposed based on wireless optical communication in visible light and infrared (IR) bands. A thorough analysis of signal-to-interference-plus-noise (SINR) is elaborated for a multi-user optical attocell network based on direct current biased optical orthogonal frequency division multiplexing (DCO-OFDM) and decode-and-forward (DF) relaying, taking into account the effects of inter-backhaul and backhaul-to-access interferences. Inspired by concepts developed for radio frequency (RF) cellular networks, full-reuse visible light (FR-VL) and in-band visible light (IB-VL) bandwidth allocation policies are proposed to realize backhauling in the visible light band. The transmission power is opportunistically minimized to enhance the backhaul power efficiency. For a two-tier FR-VL network, there is a technological challenge due to the limited capacity of the bottleneck backhaul link. The IR band is employed to add an extra degree of freedom for the backhaul capacity. For the IR backhaul system, a power-bandwidth tradeoff formulation is presented. Closed form analytical expressions are derived for the corresponding power control coefficients. Finally, the network sum rate performance is studied using extensive Monte Carlo simulations.

Index Terms—Light-fidelity (LiFi), optical attocell network, visible light communication (VLC), infrared (IR) communication, wireless backhaul, power control, multi-hop relaying, decode-and-forward (DF), direct current biased optical orthogonal frequency division multiplexing (DCO-OFDM).

I. Introduction

Nowadays light emitting diodes (LEDs) are commonly adopted for indoor illumination purposes due to their high energy efficiency, long operational lifetime and low cost. The emergence of smart environments necessitates a diversification of advanced services for light fixtures in addition to illumination [1]. A key enabler for this service diversification is visible light communication (VLC), allowing wireless communication by intensity variations of the LED light at a rate that the human eye cannot detect [1].

The growing popularity of mobile-connected devices in conjunction with ubiquitous internet access has led to an exponential increase in global mobile data traffic [2]. Fulfilling bandwidth requirements constitutes a fundamental challenge due to the scarcity of the radio frequency (RF) spectrum. The coincidence of this trend in parallel with the above

trend for LEDs has created a unique opportunity for research and development professionals to consider the visible light spectrum as a promising solution. The visible light spectrum offers a vast and unregulated bandwidth (i.e., 1000 times greater than the entire RF spectrum), which can be unlocked by means of VLC.

The application of VLC is not limited only to point-to-point communication [3]. The high speed wireless networking variant of VLC is recognized as light fidelity (LiFi) [4]. By utilizing the existing lighting infrastructure, LiFi enables LED luminaires to provide broadband wireless connectivity [4]. Due to its distinguished features such as cost effective deployment and security, LiFi will be used as a key technology in fifth generation (5G) heterogeneous wireless networks and beyond [4], [5]. The fact that more than 70% of the wireless data traffic originates inside buildings [6], makes LiFi especially advantageous for indoor applications in order to alleviate the RF spectrum crunch. Indoor networks that incorporate ultra-dense LiFi base stations (BSs) are referred to as optical attocell networks [4]. Optical attocells are tiny cells deployed with an extremely dense spatial reuse. Such cells have an equivalent circular radius between 1 m and 3 m [7]. This is analogous to long term evolution (LTE) femtocells, yet offering a much higher area spectral efficiency performance [8].

In optical intensity modulation and direct detection (IM/DD) systems, the transmitter directly modulates the intensity of the LED light. Therefore, the modulating signal is constrained to be both unipolar (i.e., non-negative) and real-valued [7]. In addition to conforming to these requirements, in order to attain high data rates with the limited communication bandwidth in VLC systems, a multi-carrier modulation scheme is preferred. The available variants of orthogonal frequency division multiplexing (OFDM) such as direct current biased optical OFDM (DCO-OFDM), asymmetrically clipped optical OFDM (ACO-OFDM) and enhanced unipolar optical OFDM (eU-OFDM) are tailored to reach a compromise for spectral efficiency and energy efficiency [7], [9], [10]. Among them, DCO-OFDM has the highest spectral efficiency and entails a relatively low implementation complexity, and this appeals to optical attocell networks [7], [11].

Backhaul is an integral part of wireless cellular networks, providing communication links to connect BSs to the core network. The backhaul quality has an unavoidable significance and impact on the overall network performance, and designing a cost effective backhaul is a major challenge for cellular networks [12]. For indoor wireless networks, there are in-building wireless backhauling technologies based on RF communications [13]. For indoor optical attocell networks,

most studies focus only on the access part, making the implicit assumption that every BS is separately equipped with an infinite capacity backhaul link to connect to the gateway, e.g., [7], [11], [14], while others use the assumption that the backhaul links are ideal (i.e., lossless and noiseless), albeit they imply a wired backhauling approach, e.g., [15], [16].

In [17], Komine and Nakagawa initially proposed the idea of exploiting the existing electricity wiring within buildings for the purpose of backhauling, leading to an integrated power line communication (PLC) and VLC system. Later, in [18], the application of a hybrid PLC-VLC system for indoor broadband broadcasting was experimentally demonstrated. Moreover, in [19], Ma *et al.* considered further optimization of the system performance using amplify-and-forward (AF) and decode-and-forward (DF) relaying for signal transmission in PLC and VLC hops. Another option for wired backhauling is Ethernet. In particular, based on the power-over-ethernet (PoE) standard, both data and electricity can be delivered to light fixtures by a single cable. In [20], Mark designed and implemented a cascaded system of PoE and VLC using a dual-hop AF relaying transmission over Ethernet and VLC hops. In addition, in [21], Delgado *et al.* designed an Ethernet-VLC interface to realize indoor broadcasting from an Ethernet-based local area network (LAN) using VLC. As an alternative to Ethernet, backhauling is also possible with optical fiber. In [22], Wang *et al.* proposed an indoor VLC-based LAN architecture where optical BSs are connected to the core network via single mode fiber links. Furthermore, to enable multi-Gbits/s connectivity based on optical fiber, the integration of a passive optical network (PON) architecture with VLC was proposed [23].

The above-mentioned backhauling approaches are all wired. A major drawback of wired solutions is that they highly depend on the wiring infrastructure where any failure directly translates into a loss on the overall network performance. Also, to enable the Ethernet solution, it is necessary to redesign the wiring infrastructure in order to distribute PoE cables to every single luminaire, incurring extra costs that scale proportionally with the network size. In addition, the optical fiber solution, though offering the highest performance, is hardly justifiable in terms of installation costs when it comes to large networks with densely deployed BSs. Moreover, the PLC installation needs additional equipment to interface between the PLC and VLC channels which introduce further complexity.

To the best of the authors' knowledge, wireless backhauling has never been considered as an option for optical attocell networks. The wireless optical backhaul solution proposed in this work makes the backhaul network independent of the wiring infrastructure. The required transceivers to establish inter-BS links are built by adding a number of low-cost LEDs and photodiodes (PDs) to LiFi BS units. In a prior study [24], for the first time, the authors have proposed and devised a wireless backhaul solution whereby the LiFi BSs are interconnected with the gateway using VLC links. In that study, a one-tier optical attocell network with a hexagonal cellular deployment was considered where each BS serves one user equipment (UE). This paper intends to take the work [24] further. By contrast, the distinct contributions of this work are

TABLE I
MATHEMATICAL NOTATIONS

Notation	Description
B_{b}	Bandwidth of the backhaul system
$x_{i,k}^{\mathrm{b}}$	Transmitted signal in the backhaul link of BS_i on subcarrier k
$y_{i,k}^{\mathrm{b}}$	Received signal for the backhaul link of BS_i on subcarrier k
$v_{i,k}^{\mathrm{b}}$	Received noise for the backhaul link of BS_i on subcarrier k
γ_{b_i}	Received SINR per subcarrier for the backhaul link of BS_i
$\mathcal{R}_{\mathrm{b}_i}$	Overall achievable rate for the backhaul link of BS_i
B_{a}	Bandwidth of the access system
$x_{i,k}^{\mathrm{a}}$	Transmitted signal in the access link of BS_i on subcarrier k
$y_{u,k}$	Received signal for the uth UE on subcarrier k
$v_{u,k}^{\mathrm{a}}$	Received noise for the uth UE on subcarrier k
γ_u	Received SINR per subcarrier for the uth UE
$\mathcal{R}_{\mathrm{a}_i}$	Overall achievable rate for the access link of BS_i
$\mathcal{R}_i$	Multi-user sum rate for the end-to-end downlink of BS_i

summarized as follows:

- The analysis is extended for a two-tier hexagonal network model using a tree topology to evaluate the scalability of the proposed backhaul solution.
- Novel analytical signal-to-noise-plus-interference ratio (SINR) expressions are derived for multi-hop DF relaying from the gateway to a UE, taking the effects of inter-backhaul and backhaul-to-access interferences into consideration.
- A multi-user scenario is considered where a given number of UEs are randomly distributed in the network.
- A power control mechanism is proposed, aiming for the optimization of the transmission power in the backhaul system. For one-tier and two-tier cases, the corresponding power allocation coefficients are derived in closed form in terms of the system parameters.
- The application of wireless infrared (IR) communication is proposed for backhauling, to enhance the performance of the backhaul system. With a power-bandwidth tradeoff analysis for a two-tier network, it is shown that a properly designed IR backhaul system can deliver the performance of an unlimited backhaul (UB) network.

A. Notations

The main mathematical notations used in this paper are listed in Table I. In addition, throughout the paper, $|\ |$ denotes the cardinality of a set; $*$ is the complex conjugate operator; $\mathbb{E}$ represents the statistical expectation; $\lfloor\ \rfloor$ is the floor function returning the largest integer that is less than or equal to its input argument; and $\preceq$ denotes the componentwise inequality.

II. SYSTEM PRELIMINARIES

Fig. 1 illustrates the geometric configuration of the downlink system in an indoor optical attocell network. The transmitter consists of a white LED installed on the ceiling and there is a solid-state PD mounted on the UE receiver. It is assumed that the LEDs are oriented vertically downward and the UE devices have a vertically upward orientation.

A. Optical Attocell Network

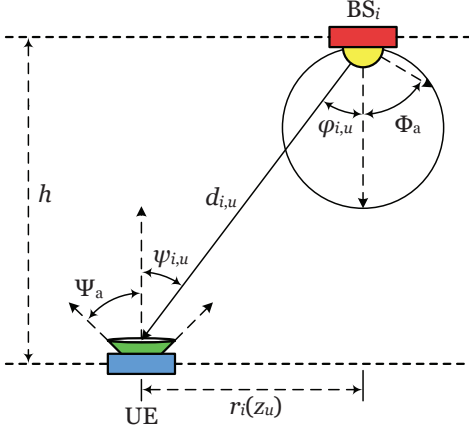An optical attocell network with a hexagonal cellular deployment is considered. Other potential deployments include

Fig. 1. Downlink geometry in an indoor optical attocell network using these parameters: Φ_{a} is the semi-angle at half-power of the Lambertian pattern; $d_{i,u}$ is the Euclidean distance between the UE and BS_i; $\varphi_{i,u}$ is the light radiance angle with respect to the normal vector of the ceiling; $\psi_{i,u}$ is the light incidence angle with respect to the normal vector of the receiver plane; Ψ_{a} is the FOV of the UE receiver; $r_i(z_u)$ is the horizontal distance between the UE and BS_i; h is the vertical distance separating the UE from the ceiling.

a square network, and a random network based on the Poisson point process (PPP) [7]. The hexagonal model gives the upper bound performance for practical optical attocell networks in terms of the SINR and cell data rate [7]. Fig. 2 depicts the layouts for a one-tier and a two-tier network, encompassing 7 and 19 attocells, respectively. There are M UEs in total in the network which are globally numbered from 1 to M. The UEs are uniformly scattered over the exact coverage of the network and they are associated with their nearest BSs according to the maximum received signal strength criterion [25], [26]. Let $\mathcal{U}_i$ be the index set of the UEs associated with BS_i such that $|\mathcal{U}_i| = M_i$ and $\sum_{i=1}^{N_{\mathrm{BS}}} M_i = M$, where N_{BS} is the total number of BSs. Each UE served by BS_i is equally given a bandwidth of $\frac{B_{\mathrm{a}}}{M_i}$, assuming a low-pass and flat frequency response for the VLC channel. The receiver field of view (FOV) is assumed to be sufficiently wide to allow simultaneous detection of optical signals from all BSs.

In this paper, a line-of-sight (LOS) light propagation model is used, as shown in Fig. 1. Note that multipath reflections due to non-line-of-sight (NLOS) paths have an insignificant effect on the attocells that are sufficiently away from the network boundaries [11]. Except in small regions near the walls, the LOS component constitutes most of the received power, i.e., more than 90% of the overall power contribution [11]. By using a Lambertian emission pattern for LEDs, the DC gain of the VLC channel from BS_i to the uth UE is given as follows [27, Eq. (10)]:

$$H_{i,u} = \frac{(m+1)A_{\mathrm{PD}}}{2\pi d_{i,u}^2}\cos^m(\varphi_{i,u})\cos(\psi_{i,u})\mathbb{1}_{\mathrm{FOV}}(\psi_{i,u}), \quad (1)$$

where $m = -\frac{\ln 2}{\ln(\cos \Phi_{\mathrm{a}})}$ is the Lambertian order and Φ_{a} is the semi-angle at half-power of the LED emission pattern; A_{PD} is the effective PD area; $d_{i,u}$ is the Euclidean distance between the UE and BS_i; $\varphi_{i,u}$ is the light radiance angle with respect to the maximum power direction for BS_i; $\psi_{i,u}$ is the light incidence angle with respect to the normal vector of the PD plane; and Ψ_{a} is the FOV for the UE receiver. These
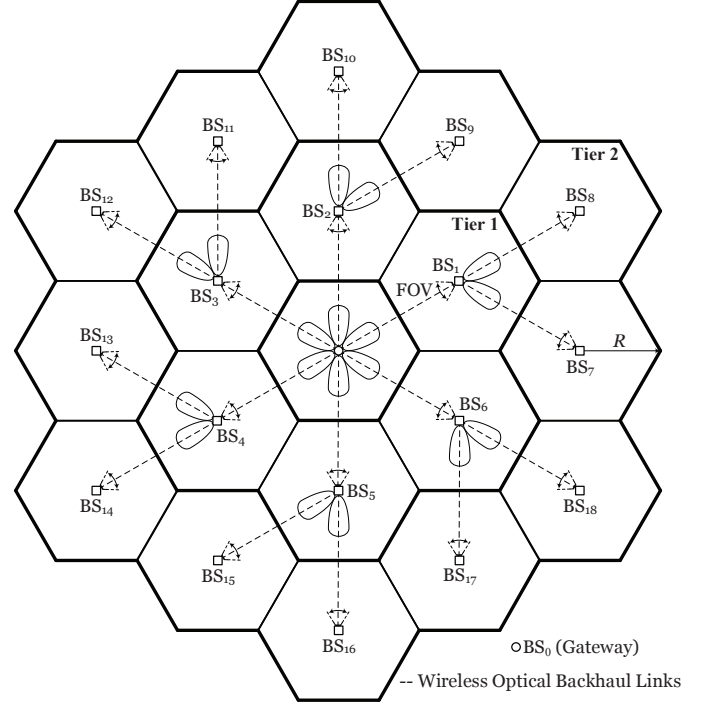
Fig. 2. Hexagonal cellular layouts for a one-tier and a two-tier optical attocell network, and a plan view of multi-hop wireless optical backhaul links.

are depicted in Fig. 1. The last factor in (1) is an indicator function defined as $\mathbb{1}_{\mathrm{FOV}}(\psi_{i,u}) = 1$ if $0 \leq \psi_{i,u} \leq \Psi_{\mathrm{a}}$, and 0 otherwise. To elaborate, a polar coordinate system with BS_0 at the origin is considered, as shown in Fig. 3. For geometric variables related to BS_0, the BS subscript 0 is dropped to simplify notation. More specifically, $z_u = (r_u, \theta_u)$ represents polar coordinates of the UE with respect to BS_0. One can express the variables $d_{i,u}$, $\cos(\varphi_{i,u})$ and $\cos(\psi_{i,u})$ in terms of $z_u = (r_u, \theta_u)$ by using the relations $d_{i,u} = \sqrt{r_i^2(z_u) + h^2}$ and $\cos(\varphi_{i,u}) = \cos(\psi_{i,u}) = \frac{h}{d_{i,u}}$, where $r_i(z_u)$ is the horizontal distance between the UE and BS_i. The polar coordinates of BS_i are denoted by (R_i, Θ_i). Assuming $0 \leq \psi_{i,u} \leq \Psi_{\mathrm{a}}$, an alternative representation is obtained for (1):

$$H_{i,u} = \frac{(m+1)h^{m+1}A_{\mathrm{PD}}}{2\pi}\left(r_i^2(z_u) + h^2\right)^{-\frac{m+3}{2}}, \quad (2)$$

where $r_i(z_u) = \sqrt{r_u^2 + R_i^2 - 2R_i r_u \cos(\theta_u - \Theta_i)}$.

The focus of this paper is primarily on the downlink. In optical attocell networks, the uplink can be realized by using IR or RF bands [3], [27], [28]. Particularly, by means of IR, and using a wavelength for the upstream direction that does not interfere with the downstream direction, both access and backhaul links can be made bidirectional. Nonetheless, the uplink is an independent problem and it is left for future works.

B. Multiple Access

In this paper, DCO-OFDM is used to realize multiple access. For each attocell, quadrature amplitude modulation (QAM) modulated symbols of the associated UEs are arranged on N subcarriers in the frequency domain. The resulting frame is of the form $\mathbf{X} = [X_0, X_1, \ldots, X_{N-1}]$, such that $X_{N-k} = X_k^*$, for $k \neq 0$. Before the application of the inverse fast Fourier

Fig. 3. Optical attocell network geometry in a polar coordinate system. An example with two UEs shows relative radial distances and polar angles.

Fig. 4. Backhaul interference caused by b_j, $j \in \mathcal{T}_1$, on the downlink of the UE associated with BS_i, $i \in \{0\} \cup \mathcal{T}_1$.

transform (IFFT), the condition $X_0 = X_{\frac{N}{2}} = 0$ has to be fulfilled in order to make the output purely real-valued. The factor $\xi = \frac{N-2}{N}$ is defined as the bandwidth utilization ratio. A cyclic prefix insertion is not considered to simplify the system model. In VLC systems, a typically short-length cyclic prefix and a single-tap equalization in the frequency domain together compensate the multipath dispersion in the channel impulse response [29]. The IFFT output signal is given by:

$$x(n) = \frac{1}{\sqrt{N}} \sum_{k=0}^{N-1} X_k \exp \left(\hat{j} \frac{2\pi k n}{N} \right), \qquad (3)$$

for $n = 0, 1, \ldots, N - 1$; and $\hat{j} = \sqrt{-1}$. The required DC bias is added in the time domain and the resulting positive signal, $\tilde{x}(n) = x(n) + x_{DC}$, drives the forward current of the LED. The DC component is given by $x_{DC} = \alpha \sqrt{P_{elec}}$, where α is a scaling factor; and P_{elec} is the total electrical power available for transmission. The DC bias controls the average optical power according to $P_{opt} = \mathbb{E}[x(n)] = x_{DC}$. Therefore, $P_{elec} = \frac{P_{opt}^2}{\alpha^2}$. Note that P_{opt} is fixed for all BSs to comply with the uniform illumination [30]. As a result, P_{elec} is constrained by the illumination requirement. In addition, P_{elec} is equally divided among data-carrying subcarriers so that each subcarrier acquires the same power of $P_a = \frac{P_{opt}^2}{(N-2)\alpha^2}$.

III. WIRELESS BACKHAUL SYSTEM DESIGN

Two configurations are investigated including a one-tier and a two-tier hexagonal network, as shown in Fig. 2. In the following, first, the modeling and analysis for a one-tier network is presented. Subsequently, the presented methodology is extended for a two-tier network.

A. Wireless Optical Backhauling

The proposed system employs point-to-point wireless optical communication so as to build a wireless backhaul network. To this end, either visible light or IR bands in the optical spectrum can be utilized, both of which are considered in this paper. There are cost-effective LED and PD devices for both bands that can be used to integrate backhaul transceivers with the BS units.

The wireless backhaul configuration using a star topology for a one-tier network is depicted in Fig. 2. As shown, only the central BS is directly connected to the core network. The remaining BSs in the first or the second tier are routed to the core network via multi-hop wireless backhaul links with the central BS using DF relaying [31]. Therefore, BS_0 is the gateway for BS_i, $\forall i \geq 1$. Relay BSs are permitted to operate in a full duplex mode because of two reasons: 1) there is no direct LOS path from the backhaul transmitter to the backhaul receiver at the same relay as they are mounted on two opposite sides of the BS unit; 2) the self-interference caused by the multipath propagation from the transmitter to the receiver on the same relay is not significant for typical indoor environments according to a study in [32]. The aim of this work is to focus on the *end-to-end* performance from the gateway to the UEs, assuming that there is a wired link between the gateway and the core network with an adequate capacity to support the aggregate data flowing in the whole backhaul network plus the downlink data for BS_0. The wireless backhaul links are provided by perfectly aligned VLC or wireless IR links. Such links can be established by adding six auxiliary LEDs on BS_0 allowing each one to point at a BS in the first tier. For each auxiliary LED, a PD is then added to the corresponding BS on the other side of the backhaul link.

The gateway continuously sends a flow of data toward BS_i without interruption. When backhaul links operate in the visible light spectrum, the access and backhaul links inevitably share the same frequency band and as a consequence, mutually interfere, assuming they are spatially transparent to each other. Note that there may be a suspended ceiling under the actual ceiling, creating an enclosed space which can physically separate the VLC channels of the access and backhaul parts. However, such a facility is not available everywhere and the purpose of this work is to avoid introducing any change to the existing indoor infrastructure. In order to manage the backhaul-to-access interference, two bandwidth allocation methods are proposed, including full reuse visible light (FR-VL) and in-band visible light (IB-VL). In the FR-VL method, the entire bandwidth is fully reused across all the access and backhaul links. In the IB-VL method, two orthog-

$$y_{1,k}^{\text{b}}(n) = R_{\text{PD}}G_{\text{b}}\sqrt{P_{\text{b}_1}}x_{1,k}^{\text{b}}(n) + R_{\text{PD}}(1/2)^{\ell}G_{\text{b}}\sqrt{P_{\text{b}_1}}\left[x_{2,k}^{\text{b}}(n) + x_{6,k}^{\text{b}}(n)\right] + v_{1,k}^{\text{b}}(n). \tag{4}$$

$$y_{u,k}^{\text{FR-VL}}(n) = R_{\text{PD}}H_{i,u}\sqrt{P_{\text{a}}}x_{i,k}^{\text{a}}(n) + R_{\text{PD}}\sum_{j\in\mathcal{Q}_i} G_{j,u}\sqrt{P_{\text{b}_j}}x_{j,k}^{\text{b}}(n) + R_{\text{PD}}\sum_{j\in\mathcal{I}_i} H_{j,u}\sqrt{P_{\text{a}}}x_{j,k}^{\text{a}}(n) + v_{u,k}^{\text{a}}(n). \tag{7}$$

---

onal sub-bands are allocated to the access and backhaul links and each sub-band may be fully reused by either one. More details are available in Section IV. For BS_i in the first tier, i.e., $i \in \mathcal{T}_1 = \{1, 2, \ldots, 6\}$, a dual-hop relaying transmission is performed over one backhaul hop and one hop for the access link. For BS_0, the entire bandwidth is fully used for downlink access even in the IB method, since BS_0 is directly connected to the gateway. Note that the access links do not affect the backhaul links based on the LOS propagation.

As an alternative to the visible light band, the IR band is considered for wireless optical backhaul design. IR LEDs typically have a much wider modulation bandwidth than white LEDs, with cutoff frequencies in the order of 440 MHz and up to 1.7 GHz [33]. Such high bandwidths are usually produced by reducing the radiative lifetime of the minority carries [34], however at the expense of decreasing the output optical power, since the internal power-bandwidth product is fixed [34]. Most commercial and low-cost IR LEDs emit wavelengths in the range between 780 nm and 950 nm [27]. The principal drawback of radiation in this range relates to eye safety, which is globally governed by international electromechanical commission (IEC) standards. In particular, the IEC Class 1 determines an allowable exposure limit for IR transmitters depending on their wavelength, diameter and emission semi-angle [27]. Also, it is desirable to limit the transmission power for IR backhauling in consideration of the power consumption.

B. Signal-to-Noise-plus-Interference Ratio

The backhaul link of BS_i, b_i, and the LED on its transmit end are both labeled with the index of the BS on its receive end. In the following, the time domain signal models are always given on subcarrier k and at time sample n, by assuming perfect sampling and synchronization. Also, it is assumed that the uth UE is associated with BS_i $\forall i \in \{0\} \cup \mathcal{T}_1$. These are not mentioned again in the sequel for the sake of brevity. Moreover, one can see in Fig. 2 that the backhaul network topology is symmetric around BS_0. Without loss of generality, the received signal model for the backhaul system is presented in terms of BS_1 and b_1.

1) Backhaul Link: For any of the proposed wireless optical backhaul systems, the signal intended for the downlink of BS_1 has to be decoded at BS_1 first. After removing the DC bias, the received signal at BS_1 from b_1 is calculated as in (4), shown at the top of the page, where R_{PD} is the PD responsivity; $G_{\text{b}} = \frac{(\ell+1)A_{\text{PD}}}{6\pi R^2}$ is the DC gain of the wireless optical channel for a backhaul link and $\ell = -\frac{\ln 2}{\ln(\cos \Phi_{\text{b}})}$ is the Lambertian order and Φ_{b} is the emission semi-angle of the auxiliary LEDs, by assuming a Lambertian emission for the auxiliary LEDs and using (1); and $v_{1,k}^{\text{b}}(n)$ is a zero mean white Gaussian noise that captures the aggregate effect of signal-independent shot noise

induced by the ambient light, and thermal noise of the receiver. The variance of $v_{1,k}^{\text{b}}(n)$ is given by $\sigma_{\text{b}}^2 = \frac{N_0 B_{\text{b}}}{N}$, where N_0 denotes the noise power spectral density (PSD). On the right hand side (RHS) of (4), $x_{2,k}^{\text{b}}(n)$ and $x_{6,k}^{\text{b}}(n)$ are interference terms caused by cross-coupling with b_2 and b_6; see Fig. 2. In (4), $P_{\text{b}_j} = K_j P_{\text{a}}$ is the power allocated to the backhaul links of the first tier, where K_j is introduced as the power control coefficient for b_j. With an equal power allocation such that $P_{\text{b}_j} = K_1 P_{\text{a}}$ $\forall j \in \mathcal{T}_1$, all the backhaul links have the same SINR. The SINR of b_j can be derived as:

$$\gamma_{\text{b}_j} = K_1\left[2\left(\frac{1}{4}\right)^{\ell}K_1 + \frac{1}{\gamma_{\text{b}}}\right]^{-1}, \ \forall j \in \mathcal{T}_1 \tag{5}$$

where:

$$\gamma_{\text{b}} = \frac{((\ell+1)A_{\text{PD}}R_{\text{PD}})^2 N P_{\text{a}}}{36\pi^2 R^4 N_0 B_{\text{b}}}. \tag{6}$$

For each backhaul system, the analysis of the downlink SINR is separately presented as follows.

2) Full Reuse Visible Light Backhaul: The received photocurrent of the uth UE situated in the attocell of BS_i, $\forall u \in \mathcal{U}_i$ and $\forall i \in \{0\} \cup \mathcal{T}_1$, can be written as in (7), shown at the top of the page, where $\mathcal{I}_i$ is the index set of interfering BSs for BS_i; $\mathcal{Q}_i$ is the index set of interfering backhaul links for BS_i; and $G_{j,u}$ represents the DC gain of the wireless optical channel between b_j and the UE. There are two types of interference on the RHS of (7). The second term is the backhaul interference and the third term is the inter-cell interference (ICI). The backhaul interference arises from the links connecting BS_0 to the first tier. Fig. 4 illustrates the backhaul interference of b_j affecting the downlink of BS_i, $\forall j \in \mathcal{T}_1$ and $\forall i \in \{0\} \cup \mathcal{T}_1$. Based on (1), one obtains $G_{j,u} = \frac{(\ell+1)A_{\text{PD}}}{2\pi d_u^2}\cos^{\ell}(\beta_{j,u})\cos(\psi_u)$, where $\beta_{j,u}$ is the light radiance angle of the auxiliary LED for b_j relative to the UE receiver. From Fig. 4, it can be observed that $\beta_{j,u}$ is related to the complementary angle $\varphi_u' = 90° - \varphi_u$ by a cylindrical rotation of $\theta_u - \Theta_j$, and therefore $\cos(\beta_{j,u}) = \cos(\varphi_u')\cos(\theta_u - \Theta_j)$, where $\cos(\varphi_u') = \frac{r_u}{d_u}$. Consequently, $G_{j,u}$ can be expressed as:

$$G_{j,u} = \frac{(\ell+1)hA_{\text{PD}}}{2\pi}r_u^{\ell}\cos^{\ell}(\theta_u - \Theta_j)(r_u^2 + h^2)^{-\frac{\ell+3}{2}}. \tag{8}$$

In (7), the variance of the noise term, $v_{u,k}^{\text{a}}(n)$, is $\sigma_{\text{a}}^2 = \frac{N_0 B_{\text{a}}}{N}$. By using (7), a unified expression is derived for the received SINR at the UE location:

$$\gamma_u^{\text{FR-VL}} = \frac{\mathcal{S}(z_u)}{\mathcal{F}_{\text{BI}}(z_u) + \mathcal{F}_{\text{ICI}}(z_u) + \Omega}, \tag{9}$$

where $\mathcal{S}(z_u)$, $\mathcal{F}_{\text{ICI}}(z_u)$ and $\mathcal{F}_{\text{BI}}(z_u)$ are defined as the desired signal effect, the ICI effect and the backhaul interference effect, respectively. The first two effects are given by:

$$\mathcal{S}(z_u) = (r_i^2(z_u) + h^2)^{-m-3}, \tag{10}$$

$$\mathcal{F}_{\mathrm{ICI}}(z_u) = \sum_{j \in \mathcal{I}_i} \left(r_j^2(z_u) + h^2 \right)^{-m-3}. \tag{11}$$

The parameter Ω in (9) is given by:

$$\Omega = \frac{4\pi^2 \alpha^2 N_0 B_{\mathrm{a}}(N-2)}{\left((m+1)h^{m+1} A_{\mathrm{PD}} R_{\mathrm{PD}} P_{\mathrm{opt}}\right)^2 N}, \tag{12}$$

Using (8), the backhaul interference effect can be derived as $\mathcal{F}_{\mathrm{BI}}(z_u) = K_1 \mathcal{F}_1(z_u; \mathcal{Q}_i)$ where $\mathcal{Q}_i \subset \mathcal{T}_1$, and:

$$\mathcal{F}_1(z_u; \mathcal{Q}_i) = \frac{(\ell+1)^2}{(m+1)^2 h^{2m}} \sum_{j \in \mathcal{Q}_i} \frac{r_u^{2\ell} \cos^{2\ell}(\theta_u - \Theta_j)}{(r_u^2 + h^2)^{\ell+3}}. \tag{13}$$

3) In-Band Visible Light Backhaul: By means of the IB-VL backhaul system, the backhaul interference effect is eliminated. From (9), the received SINR of the uth UE is readily given by:

$$\gamma_u^{\mathrm{IB\text{-}VL}} = \frac{\left(r_i^2(z_u) + h^2 \right)^{-m-3}}{\sum_{j \in \mathcal{I}_i} \left(r_j^2(z_u) + h^2 \right)^{-m-3} + \Omega}. \tag{14}$$

4) Infrared Backhaul: By employing a single IR wavelength that is fully reused across all the backhaul links, the backhaul SINR is identical to that in (5). Also, since the backhaul interference effect is perfectly canceled, the downlink SINR denoted by γ_u^{IR} is equal to $\gamma_u^{\mathrm{IB\text{-}VL}}$ given by (14).

C. Sum Rate Analysis

To facilitate the sum rate analysis, the achievable rate of a DCO-OFDM link is required in closed form. To this end, note that for a dynamic range limited wireless optical system based on DCO-OFDM, the Shannon-Hartley capacity theorem can be applied individually to each subcarrier in between two points: the input of the IFFT at the transmitter and the output of the FFT at the receiver. In principle, through a large number of subcarriers, the FFT operation effectively converts any independent and identically distributed (*i.i.d.*) perturbation term added to the received signal, including clipping noise and interference, into a Gaussian noise according to the central limit theorem [35]. In addition, there is an average power constraint to achieve the desired peak-to-average power ratio performance. Therefore, for the aforementioned input-output points *in the electrical domain*, the Shannon-Hartley capacity formula can be used. The achievable rate for a DCO-OFDM link over a flat wireless optical channel with bandwidth B is readily obtained as:

$$\mathcal{R} = \xi B \log_2 \left(1 + \gamma \right), \tag{15}$$

where γ is the received electrical SINR.

1) FR-VL Backhaul: From the definition of FR-VL backhauling, it follows that $B_{\mathrm{a}} = B_{\mathrm{b}} = B$. For BS$_0$, the sum rate of UEs can be calculated as:

$$\mathcal{R}_0^{\mathrm{FR\text{-}VL}} = \frac{\xi B}{M_0} \sum_{u \in \mathcal{U}_0} \log_2 \left(1 + \gamma_u^{\mathrm{FR\text{-}VL}} \right). \tag{16}$$

Using (5) and (9), the sum rate of UEs for BS$_i$, $\forall i \in \mathcal{T}_1$, can be expressed as:

$$\mathcal{R}_i^{\mathrm{FR\text{-}VL}} = \frac{\xi B}{M_i} \sum_{u \in \mathcal{U}_i} \log_2 \left(1 + \min \left[\gamma_{\mathrm{b}_i}, \gamma_u^{\mathrm{FR\text{-}VL}} \right] \right). \tag{17}$$

The derivation of (17) is based on [31, Eq. (15)] through setting the direct source-to-destination channel gain to zero. The factor $\frac{1}{2}$ in [31, Eq. (15)] is omitted because the relay BSs operate in full-duplex mode. In (17), $\min \left[\gamma_{\mathrm{b}_i}, \gamma_u^{\mathrm{FR\text{-}VL}} \right]$ represents the equivalent SINR of a dual-hop DF relaying transmission for the uth UE associated with BS$_i$.

2) IB-VL Backhaul: In this case, B_{a} and B_{b} correspond to two orthogonal sub-bands allocated to the access and backhaul parts. Let δ be the ratio of the bandwidth fraction allocated to the access part relative to the total VLC bandwidth. It follows that $B_{\mathrm{a}} = \delta B$ and $B_{\mathrm{b}} = (1-\delta)B$ for $0 < \delta < 1$. Considering that BS$_0$ is directly connected to the gateway, the sum rate of UEs for BS$_0$ can be equivalently represented by:

$$\mathcal{R}_0^{\mathrm{IB\text{-}VL}} = \frac{\xi B}{M_0} \sum_{u \in \mathcal{U}_0^{(\delta)}} \log_2 \left(1 + \gamma_u^{\mathrm{IB\text{-}VL}} \right) + \\ \frac{\xi B}{M_0} \sum_{u \in \mathcal{U}_0^{(1-\delta)}} \log_2 \left(1 + \gamma_u^{\mathrm{FR\text{-}VL}} \right), \tag{18}$$

where $\mathcal{U}_0^{(\delta)}$ and $\mathcal{U}_0^{(1-\delta)}$ are two complementary subsets of $\mathcal{U}_0$ such that $\left| \mathcal{U}_0^{(\delta)} \right| = \delta M_0$ and $\left| \mathcal{U}_0^{(1-\delta)} \right| = (1-\delta)M_0$, assuming δM_0 is an integer. The detailed design of δ is discussed next.

For a one-tier network, the bandwidth allocation criterion is derived as:

$$\delta \leq \frac{\log_2(1 + \gamma_{\mathrm{b}_i})}{\frac{1}{M_i} \sum_{u \in \mathcal{U}_i} \log_2(1 + \gamma_u^{\mathrm{IB\text{-}VL}}) + \log_2(1 + \gamma_{\mathrm{b}_i})}, \ \forall i \in \mathcal{T}_1 \tag{19}$$

where the equality leads to the maximum reliable rate for the dual-hop DF transmission. As the condition in (19) holds $\forall i \in \mathcal{T}_1$, among the six backhaul branches, the one with the maximum sum rate is considered to specify the value of δ. Note that once the value of δ is determined, it is fixed for the entire network. Therefore:

$$\delta = \frac{\log_2(1 + \gamma_{\mathrm{b}_1})}{\max_i \left[\frac{1}{M_i} \sum_{u \in \mathcal{U}_i} \log_2(1 + \gamma_u^{\mathrm{IB\text{-}VL}}) \right] + \log_2(1 + \gamma_{\mathrm{b}_1})}. \tag{20}$$

Based on (14) and (20), the sum rate of UEs for BS$_i$, $\forall i \in \mathcal{T}_1$, is obtained as:

$$\mathcal{R}_i^{\mathrm{IB\text{-}VL}} = \frac{\xi \delta B}{M_i} \sum_{u \in \mathcal{U}_i} \log_2 \left(1 + \gamma_u^{\mathrm{IB\text{-}VL}} \right). \tag{21}$$

Note that the methodology used here to acquire the bandwidth allocation ratio δ is consistent with that for multi-hop wireless networks using orthogonal resources for intermediate hops [36]. For example, the result presented in Lemma 1 in [36] can be derived by substituting the RHS of (19) into (21) which gives the capacity of the dual-hop system as the harmonic mean of the capacities of the two hops.

3) IR Backhaul: The IR case is similar to the FR-VL case in terms of the sum rate analysis, and the corresponding expressions for the sum rate, denoted by $\mathcal{R}_i^{\mathrm{IR}}$, can be given by (16) and (17) provided that $\gamma_u^{\mathrm{FR\text{-}VL}}$ is replaced by γ_u^{IR}.

$$y_{1,k}^{b}(n) = R_{PD}G_b\sqrt{P_{b_1}}x_{1,k}^{b}(n) + R_{PD}(1/2)^{\ell}G_b\sqrt{P_{b_1}}\left[x_{2,k}^{b}(n) + x_{6,k}^{b}(n)\right] +$$
$$R_{PD}(1/2)^{\ell+1}G_b\sqrt{P_{b_9}}x_{9,k}^{b}(n) + v_{1,k}^{b}(n). \tag{22}$$

$$y_{7,k}^{b}(n) = R_{PD}G_b\sqrt{P_{b_7}}x_{7,k}^{b}(n) + R_{PD}(1/3)\left(\sqrt{3}/2\right)^{\ell+1}G_b\sqrt{P_{b_1}}\left[x_{1,k}^{b}(n) + x_{6,k}^{b}(n)\right] +$$
$$R_{PD}(1/2)^{\ell}G_b\sqrt{P_{b_8}}x_{8,k}^{b}(n) + R_{PD}(1/2)^{\ell+1}G_b\sqrt{P_{b_8}}x_{18,k}^{b}(n) + v_{7,k}^{b}(n). \tag{23}$$

$$y_{8,k}^{b}(n) = R_{PD}G_b\sqrt{P_{b_8}}x_{8,k}^{b}(n) + R_{PD}(1/2)^{\ell}G_b\sqrt{P_{b_7}}x_{7,k}^{b}(n) +$$
$$R_{PD}(1/3)\left(\sqrt{3}/2\right)^{\ell+1}G_b\sqrt{P_{b_7}}x_{9,k}^{b}(n) + R_{PD}(5/7)\left(1/2\sqrt{7}\right)^{\ell+1}G_b\sqrt{P_{b_7}}x_{11,k}^{b}(n) + v_{8,k}^{b}(n). \tag{24}$$

IV. EXTENSION TO TWO-TIER NETWORK

The application of wireless optical backhauling is extended for a two-tier hexagonal network. Consequently, a tree topology is used for the backhaul network as shown in Fig. 2. To this end, two extra auxiliary LEDs are added to each BS in the first tier to point at two BSs in the second tier. For BS_i in the second tier, $\forall i \in \mathcal{T}_2 = \{7, 8, \ldots, 18\}$, a triple-hop relaying transmission is performed over two intermediate backhaul hops and another hop for the access link.

Due to the symmetric topology of the network around BS_0, according to Fig. 2, any one of the six backhaul branches in the tree topology is an indicator for the performance of the remaining branches. This observation especially simplifies the presentation of the received signal model for the backhaul system by focusing on BS_1, BS_7 and BS_8. First, the SINR of the backhaul links is established. Afterward, the SINR and sum rate of the downlink under different backhaul systems are individually discussed.

A. Backhaul Links

The three signals sent for the downlinks of BS_1, BS_7 and BS_8 are fully decoded at BS_1. The signal received by BS_1 through b_1 is calculated in (22), shown at the top of the page. The signals received by BS_7 and BS_8 from b_7 and b_8 are presented in (23) and (24), respectively. In (22)–(24), $P_{b_j} = K_j P_a$ is the power allocated to b_j, with K_j as the corresponding power control coefficient. An equal power is assigned to the backhaul links of the first tier. The backhaul links of the second tier are divided into two groups of odd and even-numbered, with a different power allocated to each group. This is primarily because of the asymmetric spatial distribution of the received SINR on the attocells of odd and even-numbered BSs in the second tier. The SINR of b_j can be derived and expressed as:

$$\gamma_{b_j} = K_1\left[2\left(\frac{1}{4}\right)^{\ell}K_1 + \left(\frac{1}{4}\right)^{\ell+1}K_7 + \frac{1}{\gamma_b}\right]^{-1}, \forall j \in \mathcal{T}_1 \tag{25}$$

$$\gamma_{b_j} = K_7\left[\frac{2}{9}\left(\frac{3}{4}\right)^{\ell+1}K_1 + 5\left(\frac{1}{4}\right)^{\ell+1}K_8 + \frac{1}{\gamma_b}\right]^{-1}, \forall j \in \mathcal{T}_2^{o} \tag{26}$$

$$\gamma_{b_j} = \frac{K_8}{K_7}\left[\left(\frac{1}{4}\right)^{\ell} + \frac{1}{9}\left(\frac{3}{4}\right)^{\ell+1} + \frac{25}{49}\left(\frac{1}{28}\right)^{\ell+1} + \frac{1}{K_7\gamma_b}\right]^{-1}, \forall j \in \mathcal{T}_2^{e} \tag{27}$$

where $\mathcal{T}_2^{o} = \{7, 9, \ldots, 17\}$ and $\mathcal{T}_2^{e} = \{8, 10, \ldots, 18\}$ are the index sets of odd and even-numbered BSs in the second tier, respectively.

B. FR-VL Backhaul

In a two-tier network, the downlink experiences the backhaul interference caused by both the links connecting BS_0 to the first tier and those lying in between the first and the second tiers. For the first tier, the DC gain of the interference channel, $G_{j,u}$, corresponding to b_j, $\forall j \in \mathcal{T}_1$, is given by (8). For the second tier, the calculation of $G_{j,u}$ for the downlink interference channel for b_j, $\forall j \in \mathcal{T}_2$, is similar in principle to that of (8). By contrast, the only difference comes from the need to shift the origin of the coordinate system to the coordinates of the BS in the first tier to which the transmit end of b_j is connected. Nevertheless, this is omitted here to avoid duplication. Consequently, the downlink SINR is readily available in (9) with a total backhaul interference of the form $\mathcal{F}_{BI}(z_u) = K_1\mathcal{F}_1(z_u; \mathcal{Q}_i) + K_7\mathcal{F}_2(z_u; \mathcal{O}_i) + K_8\mathcal{F}_2(z_u; \mathcal{E}_i)$, where $\mathcal{F}_1(z_u; \mathcal{Q}_i)$ is given by (13); $\mathcal{O}_i \subset \mathcal{T}_2^{o}$ and $\mathcal{E}_i \subset \mathcal{T}_2^{e}$ are the index sets of interfering odd and even-numbered backhaul links of the second tier, respectively; and:

$$\mathcal{F}_2(z_u; \mathcal{A}_i) = \frac{(\ell+1)^2}{(m+1)^2 h^{2m}}\sum_{j \in \mathcal{A}_i}\frac{r_s^{2\ell}(z_u)\cos^{2\ell}\left(\theta_s - \Theta_{b_j}\right)}{\left(r_s^2(z_i) + h^2\right)^{\ell+3}}, \tag{28}$$

for $\mathcal{A}_i = \mathcal{O}_i, \mathcal{E}_i$. In (28), (r_s, θ_s) are the relative coordinates of z_u, and Θ_{b_j} is the relative angle of b_j, with respect to the polar axis of BS_s for $s = \lfloor\frac{j-5}{2}\rfloor$.

In [24], the backhaul LED semi-angle Φ_b is identified as a key determinant of the performance for a visible light backhaul system. A special case of interest for the downlink SINR is to evaluate an asymptotic behavior of the backhaul interference effect when the wireless backhaul links are extremely directive. Such a case is used in the following as a theoretical bound for the system performance. This is established in Theorem 1.

Theorem 1. *For the FR-VL backhaul system, in the limit as Φ_b tends to zero, the backhaul interference effect on the downlink approaches zero at any location in the network, for either a one-tier or a two-tier network.*

Proof. See Appendix A. ∎

For a two-tier network, the six backhaul links branched from the gateway carry most of the data traffic in the network, and each one has to accommodate three downstream data flows. In order to fairly apportion the backhaul capacity, an equally

$$\mathcal{R}_i^{\text{FR-VL}} = \frac{\xi B}{M_i} \sum_{u \in \mathcal{U}_i} \min \left[\mu_i \log_2 \left(1 + \gamma_{\text{b}_i} \right), \log_2 \left(1 + \gamma_u^{\text{FR-VL}} \right) \right], \ \forall i \in \mathcal{T}_1 \tag{29}$$

$$\mathcal{R}_i^{\text{FR-VL}} = \frac{\xi B}{M_i} \sum_{u \in \mathcal{U}_i} \min \left[\mu_i \log_2 \left(1 + \gamma_{\text{b}_s} \right), \log_2 \left(1 + \gamma_{\text{b}_i} \right), \log_2 \left(1 + \gamma_u^{\text{FR-VL}} \right) \right], \ \forall i \in \mathcal{T}_2 \tag{30}$$

weighted fair scheduling method is employed [37], by which every data flow in a shared backhaul link is allocated an equal proportion of the available capacity. The allocated resources are orthogonal so that b_1 is effectively decomposed into three independent parallel channels, each one having an achievable rate of $\mu_j \mathcal{R}_{\text{b}_1}$, where $\mu_j = \frac{1}{3}$ is the weight assigned to the jth data flow. The capacity of b_1 can be decomposed in the frequency domain. According to μ_j, the DCO-OFDM frame is divided into three parts and each one is independently loaded with an information block from the jth data flow. At BS_1, different sub-bands are separated in the frequency domain based on the FFT of the received signal. Once the symbols encapsulated in the three sub-bands are individually decoded, each group is modulated with a distinct OFDM frame which is retransmitted in the corresponding direction. Furthermore, for the first and the second tiers, the end-to-end rate of UEs cannot be higher than the allocated capacity of each intermediate hop based on the maximum flow–minimum cut theorem [38]. By using (25)–(27) and (9), the sum rate of UEs for BS_i, is derived as in (29) for $i \in \mathcal{T}_1$, and in (30) for $i \in \mathcal{T}_2$, where $s = \lfloor \frac{i-5}{2} \rfloor$.

C. IB-VL Backhaul

For a two-tier network, the bandwidth allocation ratio δ is upper bounded as follows:

$$\delta \leq \frac{\log_2(1 + \gamma_{\text{b}_i})}{\sum_{j \in \mathcal{L}_i} \frac{1}{M_j} \sum_{u \in \mathcal{U}_j} \log_2(1 + \gamma_u^{\text{IB-VL}}) + \log_2(1 + \gamma_{\text{b}_i})}, \ \forall i \in \mathcal{T}_1 \tag{31}$$

where $\mathcal{L}_i = \{i, 2i+5, 2i+6\} \ \forall i \in \mathcal{T}_1$. The minimum value for δ is obtained by taking the maximum sum rate over the six possible triples on the RHS of (31), corresponding to the six backhaul branches. The value of δ is fixed to be:

$$\delta = \frac{\log_2(1 + \gamma_{\text{b}_1})}{\max_i \left[\sum_{j \in \mathcal{L}_i} \frac{1}{M_j} \sum_{u \in \mathcal{U}_j} \log_2(1 + \gamma_u^{\text{IB-VL}}) \right] + \log_2(1 + \gamma_{\text{b}_1})}. \tag{32}$$

Based on (32), the sum rate of UEs for BS_i, $\forall i \in \mathcal{T}_1 \cup \mathcal{T}_2$, is readily given by (21).

Note that the number of orthogonal resources in this work (i.e., sub-bands) is always two, unlike the case in [36] where the number of orthogonal resources is equal to the number of hops in the network (i.e., half-duplex). In particular, there are only two orthogonal sub-bands for a two-tier network in which three hops are involved for downlink transmission in the second tier.

D. IR Backhaul

Under the assumption of a single IR wavelength being fully reused over all the backhaul links, the sum rates in (29) and

(30) for the FR-VL case apply to the IR case, $\mathcal{R}_i^{\text{IR}}$, upon substituting $\gamma_u^{\text{FR-VL}}$ with γ_u^{IR}.

V. POWER CONTROL FOR WIRELESS BACKHAUL SYSTEM

A power optimization framework is presented for wireless optical backhaul systems discussed in Sections III and IV. This is particularly motivated by the fact that backhaul LEDs do not need to provide illumination for the environment, and their optical power can therefore be minimized to enhance the power efficiency. However, reducing the power in the backhaul links adversely affects their capacity, and thus the network performance may be compromised. Finding the minimum power for the backhaul system while maintaining the network performance at a desired level is formulated as an optimization problem. Note that P_{a} is already fixed. As a result, the minimization of P_{b_j} is equivalent to the minimization of $K_j = \frac{P_{\text{b}_j}}{P_{\text{a}}}$. Due to eye safety considerations, the allowed peak power for all wireless optical backhaul systems is limited to be no more than the power of the access system, as the backhaul LEDs may have narrow emission semi-angles. This means $P_{\text{b}_j} \leq P_{\text{a}}$, and hence $0 < K_j \leq 1 \ \forall j$. Note that $K_j = 1$ represents the case where no power control is applied to b_j.

In order to adjust the backhaul power, the network controller requires the instantaneous channel state information for each UE individually. However, for large networks with a large number of UEs, fulfilling such a requirement is cumbersome and practically infeasible. Hence, a scenario in which every BS experiences the highest sum rate from the associated UEs is considered, implying the highest load on the backhaul system. In a given attocell, the maximum achievable rate coincides with the unique point where the peak SINR occurs. Obviously, the sum rate of multiple UEs all of which are colocated at such a point is equal to the achievable rate of a single UE located at the same point, assuming a uniform bandwidth allocation to UEs. Therefore, it is sufficient to focus on the point that corresponds to the peak SINR for the purpose of optimization, and the UE index u is dropped. Although the described scenario might be the worst case, the advantages include: 1) there is no need for the knowledge of the instantaneous downlink channel; 2) the power optimization is done only once for a given network configuration.

In the following, the backhaul power optimization is presented first for a one-tier network and then for a two-tier network. To elaborate, let z_i represent an arbitrary point within the attocell of BS_i with γ_i denoting the downlink SINR at z_i and let $z_{i,\max} = (r_{i,\max}, \theta_{i,\max})$ be the point of the maximum downlink SINR.

A. One-Tier Network

To avoid restricting the achievable rate in the downlink, an adequate capacity is required for the backhaul system. For a one-tier network, the backhaul-access rate constraint is:

$$\mathcal{R}_{b_1} \geq \mathcal{R}_{a_1}. \tag{33}$$

1) FR-VL Backhaul:
The optimization problem is stated as follows:

$$\text{P1}: \underset{K_1}{\text{minimize}} \quad K_1$$
$$\text{subject to} \quad \log\left(1 + \gamma_{b_1}\right) - \log\left(1 + \gamma_1^{\text{FR-VL}}\right) \geq 0,$$
$$0 < K_1 \leq 1. \tag{34}$$

The first constraint is due to (33). The second constraint is to limit the backhaul power to be always less than or equal to the access power. The first constraint can be equivalently written as $\gamma_{b_1} \geq \gamma_1^{\text{FR-VL}}$. Using (9)–(13) for $i = 1$ in place of $\gamma_1^{\text{FR-VL}}$, and solving the inequality for K_1, one obtains:

$$K_1 \geq K_{1,\min}, \tag{35}$$

where $K_{1,\min}$ is derived in closed form:

$$K_{1,\min} = \frac{\mathcal{S}(z_1)}{2\mathcal{F}_1(z_1; \mathcal{Q}_1)} \left[-\frac{\mathcal{F}_{\text{ICI}}(z_1) + \Omega}{\mathcal{S}(z_1)} + 2\left(\frac{1}{4}\right)^\ell + \sqrt{\left(\frac{\mathcal{F}_{\text{ICI}}(z_1) + \Omega}{\mathcal{S}(z_1)} - 2\left(\frac{1}{4}\right)^\ell\right)^2 + \frac{4\mathcal{F}_1(z_1; \mathcal{Q}_1)}{\mathcal{S}(z_1)\gamma_b}} \right]. \tag{36}$$

Note that $K_{1,\min}$ is expressed at $z_1 = (r_1, \theta_1)$ which can be anywhere within the attocell of BS_1. At the same time, finding exact coordinates of $z_{1,\max}$ depends on the value of K_1. One can jointly find the values of $K_{1,\min}$ and $z_{1,\max}$ by using (36) and maximizing $\gamma_1^{\text{FR-VL}}$ given by (9), in a recursive manner. For infinite size attocell networks, the received SINR peaks exactly at the center of each attocell [7]. It might slightly deviate from the center due to the finite network deployment and the backhaul interference effect. The approximation $z_{1,\max} \approx (0,0)$ is used for simplicity. The solution to P1 can be written in the form:

$$K_1^* = \min[K_{1,\min}, 1]. \tag{37}$$

Numerical results are mainly presented in terms of the backhaul LED semi-angle given a fixed configuration for the downlink system. In optical attocell networks, the downlink parameters such as the LED semi-angle, cell coverage radius and vertical separation are essentially configured to meet the requirements for illumination and SINR quality [7]. Table II lists the system parameters used for simulations.

Fig. 5 shows the optimal solution K_1^* to P1 against Φ_b. It can be observed that by increasing Φ_b, the value of K_1^* is saturated at unity for $\Phi_b \geq 35°$. The value of K_1^* stays below 0.1 for $\Phi_b \leq 25°$. In this case, the power allocated to the backhaul links can be less than one tenth of the downlink power which is a remarkable gain for power efficiency of the FR-VL backhaul system.

TABLE II
SYSTEM PARAMETERS

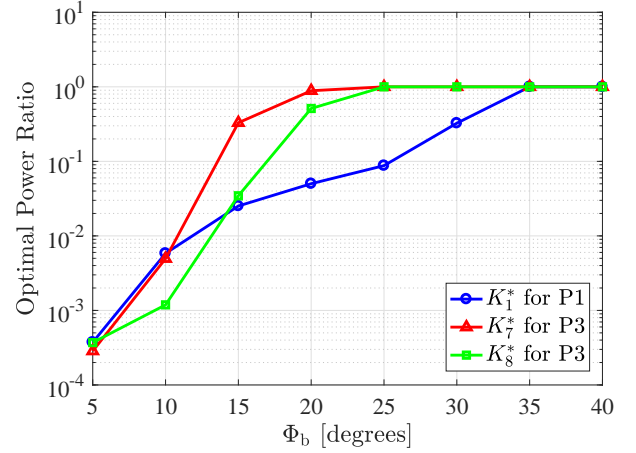| Parameter	Symbol	Value
Downlink LED Optical Power	P_{opt}	10 W
Downlink LED Semi-Angle	Φ_a	40°
Vertical Separation	h	2.25 m
Hexagonal Cell Radius	R	2.5 m
Total VLC Bandwidth	B	20 MHz
IFFT/FFT Length	N	1024
Noise Power Spectral Density	N_0	10^{-21} A^2/Hz
Receiver Field of View	Ψ_a, Ψ_b	85°
PD Effective Area	A_{PD}	10^{-4} m^2
PD Responsivity	R_{PD}	0.6 A/W
DC Bias Scaling Factor	α	3

Fig. 5. Optimal power ratios K_1^* for the one-tier FR-VL network, and K_7^* and K_8^* for the two-tier FR-VL network with respect to Φ_b.

2) IR Backhaul and Power-Bandwidth Tradeoff:
The bandwidth of the IR system is taken as a variable. More specifically, the desired variable is defined as the ratio of the bandwidth of the backhaul system to that of the downlink system, i.e., $\frac{B_b}{B_a}$. The optimization problem statement is similar to the FR-VL case and is omitted to avoid duplication. The minimum power ratio $K_{1,\min}$ satisfies the constraint in (33), and it can be derived by substituting $\mathcal{R}_{b_1} = \xi B_b \log_2(1 + \gamma_{b_1})$ and $\mathcal{R}_{a_1} = \xi B_a \log_2\left(1 + \gamma_1^{\text{IR}}\right)$ into (33), which gives:

$$K_{1,\min} = \frac{\left[\left(\left(1 + \gamma_1^{\text{IR}}\right)^{\frac{B_a}{B_b}} - 1\right)^{-1} - 2\left(\frac{1}{4}\right)^\ell\right]^{-1}}{\gamma_b}. \tag{38}$$

Fig. 6 presents $K_{1,\min}$ as a function of $\frac{B_b}{B_a}$ for different values of Φ_b. A tradeoff is observed between the minimum power ratio and the required bandwidth ratio. The tradeoff is improved by focusing the light beam in the backhaul links. For $\frac{B_b}{B_a} = 1$, $K_{1,\min} < 1$ for all considered values of Φ_b. Fig. 7 shows the optimal power ratio, defined as $K_1^* = [K_{1,\min}, 1]$, with respect to Φ_b for different values of B_b. It can be seen that the optimal power ratio is an increasing function of Φ_b. Also, it can be observed that increasing B_b provides a higher improvement for the optimal power ratio in lower bandwidths. For example, consider increasing B_b from B_a to $3B_a$ and that from $10B_a$ to $20B_a$. The justification is that by increasing B_b, the reduction rate of $K_{1,\min}$ diminishes for higher values of the bandwidth according to Fig. 6.
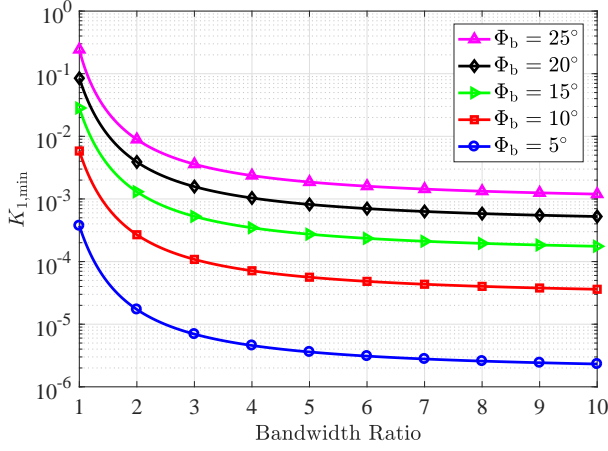
Fig. 6. The minimum power ratio $K_{1,\text{min}}$ against the bandwidth ratio $\frac{B_b}{B_a}$ for the one-tier network with IR backhaul.

Fig. 7. Optimal power ratio K_1^* for the one-tier network with IR backhaul versus Φ_b for different values of B_b.

B. Two-Tier Network

For a two-tier network, there are three backhaul-access rate constraints of:

$$\mathcal{R}_{b_1} \geq \mathcal{R}_{a_1} + \mathcal{R}_{a_7} + \mathcal{R}_{a_8}, \tag{39}$$

$$\mathcal{R}_{b_7} \geq \mathcal{R}_{a_7}, \tag{40}$$

$$\mathcal{R}_{b_8} \geq \mathcal{R}_{a_8}. \tag{41}$$

Among (39)–(41), (39) is the dominant constraint, meaning that the capacity of b_1 has to be sufficiently high to support the aggregate rate demanded by BS_1, BS_7 and BS_8. Otherwise, the limited capacity of b_1 turns into a backhaul bottleneck.

1) FR-VL Backhaul: The optimization problem is stated as follows:

$$
\begin{aligned}
\text{P2}: \quad & \underset{\{K_1, K_7, K_8\}}{\text{minimize}} \quad K_{\text{sum}} = \sum_{j=1,7,8} K_j \\
& \text{subject to} \quad g_1(K_1, K_7, K_8) \geq 0, \\
& \qquad \log(1 + \gamma_{b_7}) - \log\left(1 + \gamma_7^{\text{FR-VL}}\right) \geq 0, \\
& \qquad \log(1 + \gamma_{b_8}) - \log\left(1 + \gamma_8^{\text{FR-VL}}\right) \geq 0, \\
& \qquad 0 < K_j \leq 1.
\end{aligned}
\tag{42}
$$

The objective is to minimize the total power allocated to each backhaul branch including three backhaul links. The first three constraints are adopted from (39)–(41). The function g_1 in the first constraint is given by:

$$g_1(K_1, K_7, K_8) = \log(1 + \gamma_{b_1}) - \sum_{i=1,7,8} \log\left(1 + \gamma_i^{\text{FR-VL}}\right). \tag{43}$$

An instant illustration of the admissible region defined by the first three constraints in (42) helps to gain insight on the solution space for P2. To this end, note that the function g_1 in (43) is monotonically increasing in the direction of K_1. It is shown in Appendix B that the partial derivative of g_1 with respect to K_1 is strictly positive. Therefore, one can rearrange the first constraint in (42) and write it as:
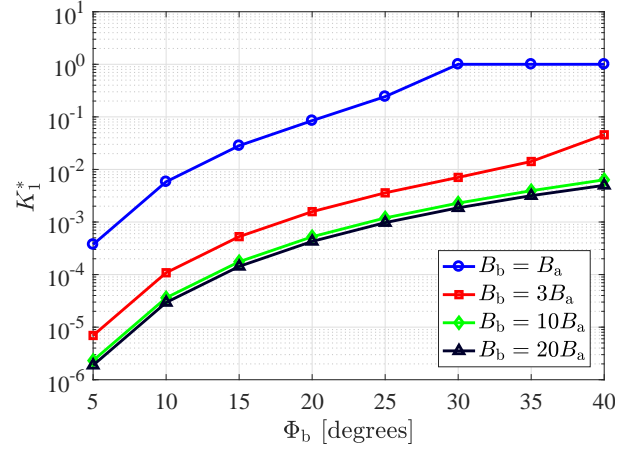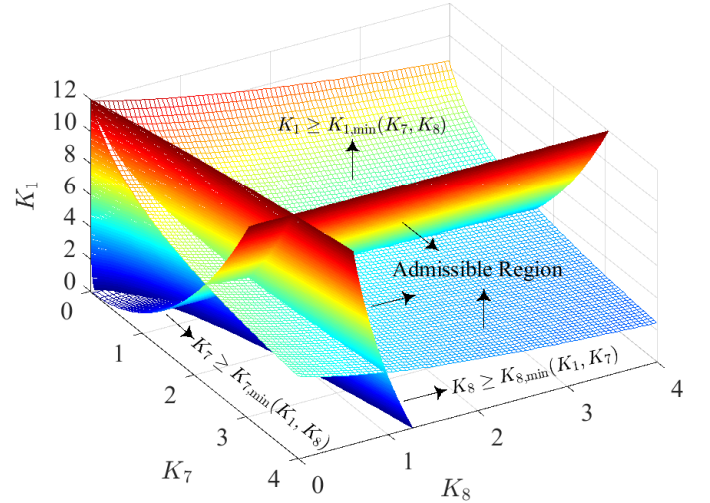
$$K_1 \geq K_{1,\text{min}}(K_7, K_8). \tag{44}$$

Fig. 8. An instant illustration of the admissible region for P2 based on the first three constraints for $\Phi_b = 20°$.

In a similar way, the following alternative forms are obtained for the second and the third constraints in (42), respectively:

$$K_7 \geq K_{7,\text{min}}(K_1, K_8), \tag{45}$$

$$K_8 \geq K_{8,\text{min}}(K_1, K_7), \tag{46}$$

where $K_{7,\text{min}}(K_1, K_8)$ and $K_{8,\text{min}}(K_1, K_7)$ are derived in closed from in (47) and (48), shown at the top of the next page, respectively. However, $K_{1,\text{min}}$ in (44) cannot be explicitly expressed in terms of K_7 and K_8, as the equation $g_1(K_1, K_7, K_8) = 0$ is non-resolvable for K_1. The Newton-Raphson method is used to evaluate $K_{1,\text{min}}(K_7, K_8)$ given the values of K_7 and K_8, according to the following iterative rule:

$$K_{1,\text{min}}^{(n)} = K_{1,\text{min}}^{(n-1)} - \left. \frac{g_1(K_1, K_7, K_8)}{\frac{\partial g_1}{\partial K_1}} \right|_{K_1 = K_{1,\text{min}}^{(n-1)}}, \tag{49}$$

where the superscript n indicates the iteration number. Fig. 8 illustrates the boundary surfaces for (44), (45) and (46), for $\Phi_b = 20°$. It is observed that the boundary surface of $K_{1,\text{min}}(K_7, K_8)$ stands beyond the allowed level of $K_1 = 1$.

$$K_{7,\min}(K_1, K_8) = \frac{\mathcal{S}(z_7)}{2\mathcal{F}_2(z_7; \mathcal{O}_7)} \left[-\frac{K_1 \mathcal{F}_1(z_7; \mathcal{Q}_7) + K_8 \mathcal{F}_2(z_7; \mathcal{E}_7) + \mathcal{F}_{\text{ICI}}(z_7) + \Omega}{\mathcal{S}(z_7)} + \right. \tag{47}$$

$$\left. \left(\left(\frac{K_1 \mathcal{F}_1(z_7; \mathcal{Q}_7) + K_8 \mathcal{F}_2(z_7; \mathcal{E}_7) + \mathcal{F}_{\text{ICI}}(z_7) + \Omega}{\mathcal{S}(z_7)} \right)^2 + \right. \right.$$

$$\left. \left. \frac{4\mathcal{F}_2(z_7; \mathcal{O}_7)}{\mathcal{S}(z_7)} \left(\frac{2}{9} \left(\frac{3}{4} \right)^{\ell+1} K_1 + 5 \left(\frac{1}{4} \right)^{\ell+1} K_8 + \frac{1}{\gamma_{\text{b}}} \right) \right)^{\frac{1}{2}} \right].$$

$$K_{8,\min}(K_1, K_7) = \frac{\mathcal{S}(z_8)}{2\mathcal{F}_2(z_8; \mathcal{E}_8)} \left[-\frac{K_1 \mathcal{F}_1(z_8; \mathcal{Q}_8) + K_7 \mathcal{F}_2(z_8; \mathcal{O}_8) + \mathcal{F}_{\text{ICI}}(z_8) + \Omega}{\mathcal{S}(z_8)} + \right. \tag{48}$$

$$\left. \left(\left(\frac{K_1 \mathcal{F}_1(z_8; \mathcal{Q}_8) + K_7 \mathcal{F}_2(z_8; \mathcal{O}_8) + \mathcal{F}_{\text{ICI}}(z_8) + \Omega}{\mathcal{S}(z_8)} \right)^2 + \right. \right.$$

$$\left. \left. \frac{4\mathcal{F}_2(z_8; \mathcal{E}_8)}{\mathcal{S}(z_8)} \left(\left[\left(\frac{1}{4} \right)^{\ell} + \frac{1}{9} \left(\frac{3}{4} \right)^{\ell+1} + \frac{25}{49} \left(\frac{1}{28} \right)^{\ell+1} \right] K_7 + \frac{1}{\gamma_{\text{b}}} \right) \right)^{\frac{1}{2}} \right].$$

Moreover, when considering the three boundaries, their admissible region has no intersection with the unit cube defined by the last constraint in (42). This reveals a fundamental design challenge for the FR-VL backhaul system since the power in the backhaul links is not practically allowed to exceed the downlink power, and thus the finite capacity of b_i, $i \in \mathcal{T}_1$, determines the upper limit of the downlink data rate in the first and the second tiers. In fact, the feasible set of P2 is empty for most practical cases. To verify this observation, the feasibility of the constraint in (44) has to be examined analytically. However, the function $K_{1,\min}(K_7, K_8)$ is not available in closed form. Instead, an asymptotic bound is derived for $K_{1,\min}(K_7, K_8)$ for small values of Φ_{b} in Appendix C. This bound represents the best scenario under which the backhaul links attain a high capacity by means of focusing the light emission pattern. In practice, this can be realized by using appropriate optical lenses to collimate the LED light in the backhaul links. Based on (64), and using the system parameters in Table II, it can be verified that $K_{1,\min} \gg 1$. For example, $K_{1,\min} \approx 480$ for $\Phi_{\text{b}} = 5°$. To move on further, the first constraint is relaxed by fixing K_1 at $K_1 = 1$, which is the maximum possible value for K_1. One can continue to minimize K_7 and K_8 with the new problem stated as follows:

$$\text{P3}: \min_{\{K_7, K_8\}} \quad \sum_{j=7,8} K_j$$

$$\text{subject to} \quad K_7 \geq K_{7,\min}(K_8), \tag{50}$$
$$K_8 \geq K_{8,\min}(K_7),$$
$$0 < K_j \leq 1.$$

Fig. 9 illustrates the admissible region for P3 for $\Phi_{\text{b}} = 20°$ on the K_7-K_8 plane, based on the boundaries given by (47) and (48) for $K_1 = 1$. It can be verified that the boundary curves $K_{7,\min}(K_8)$ and $K_{8,\min}(K_7)$ are monotonically increasing for $K_7 > 0$ and $K_8 > 0$. They coincide at the unique intersection point represented by $\left(K_{7,\min}^{\dagger}, K_{8,\min}^{\dagger} \right)$ in the positive quadrant $\mathbb{R}_+^2$, which, in fact, is the minimum
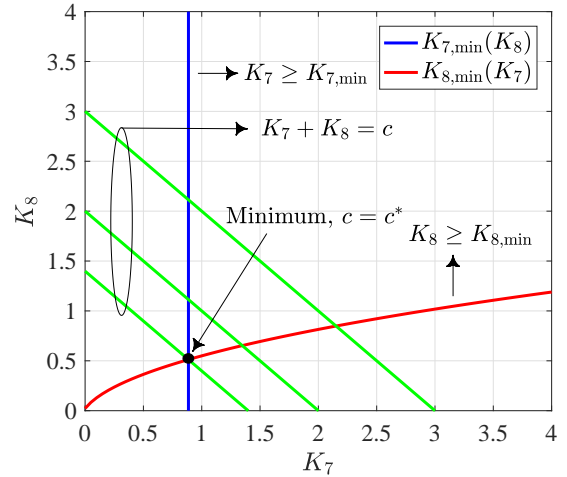

Fig. 9. An instant illustration of the admissible region for P3 for $\Phi_{\text{b}} = 20°$. The objective function is shown as the family of lines $K_7 + K_8 = c$ for three values of c. The minimum of the objective function is indicated by $c = c^*$.

element of the feasible set. This is proved by using the aforementioned property of the boundary curves; see Appendix D. The projections of the objective function onto the K_7-K_8 plane are the family of lines $K_7 + K_8 = c$ for $c \geq 0$, as shown for different values of c in Fig. 9. By decreasing c, the minimum value of the objective function occurs for $c = c^*$ at the intersection point. The solution to P3 can be written as:

$$(K_7^*, K_8^*) = \left(\min \left[K_{7,\min}^{\dagger}, 1 \right], \min \left[K_{8,\min}^{\dagger}, 1 \right] \right). \tag{51}$$

Referring to Fig. 5, the optimal solutions (K_7^*, K_8^*) to P3 against Φ_{b} are shown. It can be observed that by increasing Φ_{b}, the value of K_1^* is saturated at unity for $\Phi_{\text{b}} \geq 35°$. It is observed that for $\Phi_{\text{b}} \leq 20°$, both K_7^* and K_8^* are less than one. The power minimization for the FR-VL backhaul system in the two-tier case encountered a fundamental limitation due to the inadequate capacity of the bottleneck backhaul link even
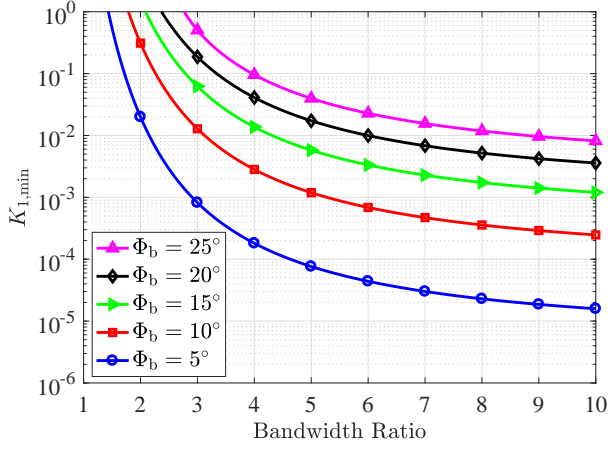
Fig. 10. The tradeoff between the minimum power ratio $K_{1,\min}$ and the bandwidth ratio $\frac{B_b}{B_a}$ for the two-tier network with IR backhaul.

Fig. 11. The minimum bandwidth ratio $\frac{B_b}{B_a}\big|_{\min}$ against Φ_b for the two-tier network with IR backhaul for different values of $K_{1,\min}$.

when using a directive light beam. This challenge is addressed by using the IR band for backhauling.

2) IR Backhaul and Power-Bandwidth Tradeoff: Different from the FR-VL case, for the IR case, the underlying optimization problem for a two-tier network can be solved. The reason for this is the downlink SINR γ_1^{IR} does not depend on the power ratios unlike in the FR-VL case. Therefore, γ_1^{IR} is decoupled from γ_{b_1}, and this causes the boundary surface defined by (39), i.e., $K_{1,\min}(K_7, K_8)$, to be a flat plane. By considering the other two planes defined by (40) and (41), i.e., $K_{7,\min}(K_1, K_8)$ and $K_{8,\min}(K_1, K_7)$, the solution is at the vertex of the admissible region, which is the intersection of the three planes. Based on (39), $K_{1,\min}$ is derived in (52), shown at the top of the next page. Based on the other two constraints in (40) and (41), and by using (52), the minimum power ratios $K_{7,\min}$ and $K_{8,\min}$ are derived in (53) and (54), respectively. Among the three power ratios of $K_{1,\min}$, $K_{7,\min}$ and $K_{8,\min}$, $K_{1,\min}$ introduces the most challenging tradeoff as it represents the bottleneck backhaul link.

Fig. 10 demonstrates the tradeoff between $K_{1,\min}$ and $\frac{B_b}{B_a}$ for the same set of values for Φ_b as used in Fig. 6. Compared with Fig. 6, the tradeoff curves are shifted to the right. In particular, so as to achieve $K_{1,\min} < 1$, a bandwidth ratio of $\frac{B_b}{B_a} > 1$ is required even in the case where Φ_b is as small as $5°$. As a design guideline, it is useful to investigate how much bandwidth is needed for the IR backhaul system to ensure a certain minimum power level for the bottleneck backhaul link. This can be acquired using Fig. 10. For instance, to allow the power ratio of the bottleneck backhaul link to be equal to $K_{1,\min} = 0.01$ for $\Phi_b = 5°$, a bandwidth ratio no less than $\frac{B_b}{B_a} = 2.1$ is needed. The minimum bandwidth ratio denoted by $\frac{B_b}{B_a}\big|_{\min}$ is formally presented in Fig. 11 as a function of Φ_b for different values of $K_{1,\min}$. It can be observed that $\frac{B_b}{B_a}\big|_{\min}$ is rising with increase in Φ_b. The case of $K_{1,\min} = 1$ gives the lower bound for the minimum bandwidth ratio. For $\Phi_b = 20°$, $\frac{B_b}{B_a}\big|_{\min} = 6, 3.3, 2.4$ for $K_{1,\min} = 0.01, 0.1, 1$.

Fig. 12 presents the optimal sum power ratio defined as $K_{\text{sum}} = K_1^* + K_7^* + K_8^*$ against Φ_b for different values of B_b, where $K_j^* = \min[K_{j,\min}, 1]$ for $j = 1, 7, 8$. Note that the
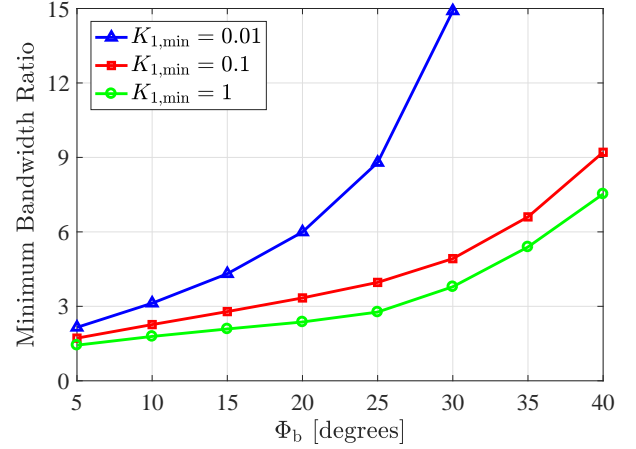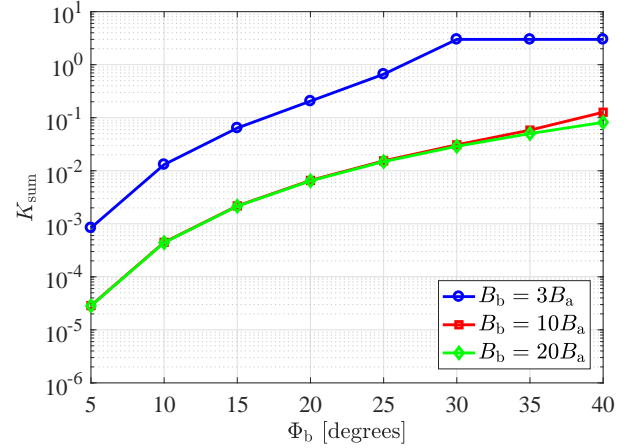

Fig. 12. Optimal sum power ratio $K_{\text{sum}} = K_1^* + K_7^* + K_8^*$ for the two-tier network with IR backhaul versus Φ_b for different values of B_b.

maximum value of K_{sum} is exactly equal to 3, which can be seen in the case of $B_b = 3B_a$ in Fig. 12. It can be observed that by further increasing the bandwidth after $B_b = 10B_a$, there is a negligible change in K_{sum}. This can be explained as the values of K_j^* are effectively flattened for $B_b \geq 10B_a$.

Next, simulation results are presented for the overall average sum rate performance of one-tier and two-tier optical attocell networks using FR-VL, IB-VL and IR backhaul systems based on the sum rate analysis and the backhaul power optimization presented in Sections IV and V. In addition, a UB network is considered as the baseline scenario in which every single BS is individually connected to the core network using a high capacity wired backhaul link. Simulations are conducted based on Monte Carlo averaging over a large number of random realizations for the distribution of UEs in the network, using the parameters given in Table II. To make a fair comparison between a one-tier and a two-tier network, the average UE density (i.e., the average number of UEs per cell) is fixed, by considering $M = 15$ and $M = 40$ for one-tier and two-tier cases, respectively. For FR-VL and IR backhaul systems, both cases including with and without power control are studied using various combinations of the power ratios to exemplify

$$K_{1,\min} = \left[\prod_{i=7,8} \left[\left(1 + \gamma_i^{\text{IR}}\right)^{\frac{B_a}{B_b}} - 1 \right]^{-1} + \left(\frac{1}{4}\right)^{\ell+1} \left[\left(1 + \gamma_8^{\text{IR}}\right)^{\frac{B_a}{B_b}} - 1 \right]^{-1} - \right.$$
$$\left. 5 \left(\frac{1}{4}\right)^{\ell+1} \left[\frac{3}{4}\left(\frac{1}{4}\right)^{\ell} + \frac{1}{9}\left(\frac{3}{4}\right)^{\ell+1} + \frac{25}{49}\left(\frac{1}{28}\right)^{\ell+1} \right] \right] \gamma_b^{-1} \Delta^{-1}, \tag{52}$$

$$K_{7,\min} = \left[\left(\left[\prod_{i=1,7,8} \left(1 + \gamma_i^{\text{IR}}\right)^{\frac{B_a}{B_b}} - 1 \right]^{-1} - 2\left(\frac{1}{4}\right)^{\ell} \right) \left(\left[\left(1 + \gamma_8^{\text{IR}}\right)^{\frac{B_a}{B_b}} - 1 \right]^{-1} + \right. \right.$$
$$\left. \left. 5 \left(\frac{1}{4}\right)^{\ell+1} \right) + \frac{2}{9}\left(\frac{3}{4}\right)^{\ell+1} \left[\left(1 + \gamma_8^{\text{IR}}\right)^{\frac{B_a}{B_b}} - 1 \right]^{-1} \right] \gamma_b^{-1} \Delta^{-1}, \tag{53}$$

$$K_{8,\min} = \left[\left(\left[\prod_{i=1,7,8} \left(1 + \gamma_i^{\text{IR}}\right)^{\frac{B_a}{B_b}} - 1 \right]^{-1} - 2\left(\frac{1}{4}\right)^{\ell} \right) \left(\left[\left(1 + \gamma_7^{\text{IR}}\right)^{\frac{B_a}{B_b}} - 1 \right]^{-1} + \left(\frac{1}{4}\right)^{\ell} + \right. \right.$$
$$\left. \frac{1}{9}\left(\frac{3}{4}\right)^{\ell+1} + \frac{25}{49}\left(\frac{1}{28}\right)^{\ell+1} \right) + \frac{2}{9}\left(\frac{3}{4}\right)^{\ell+1} \left[\frac{3}{4}\left(\frac{1}{4}\right)^{\ell} + \frac{1}{9}\left(\frac{3}{4}\right)^{\ell+1} + \frac{25}{49}\left(\frac{1}{28}\right)^{\ell+1} \right] \right] \gamma_b^{-1} \Delta^{-1}, \tag{54}$$

$$\Delta = \left(\prod_{i=7,8} \left[\left(1 + \gamma_i^{\text{IR}}\right)^{\frac{B_a}{B_b}} - 1 \right]^{-1} - 5\left(\frac{1}{4}\right)^{\ell+1} \left[\left(\frac{1}{4}\right)^{\ell} + \frac{1}{9}\left(\frac{3}{4}\right)^{\ell+1} + \frac{25}{49}\left(\frac{1}{28}\right)^{\ell+1} \right] \right) \times$$
$$\left(\left[\prod_{i=1,7,8} \left(1 + \gamma_i^{\text{IR}}\right)^{\frac{B_a}{B_b}} - 1 \right]^{-1} - 2\left(\frac{1}{4}\right)^{\ell} \right) - \frac{2}{9}\left(\frac{3}{16}\right)^{\ell+1} \left[\left(1 + \gamma_8^{\text{IR}}\right)^{\frac{B_a}{B_b}} - 1 \right]^{-1}. \tag{55}$$

the effect of power control on the network performance. Note that the optimization objective is the sum power of the backhaul system and therefore it does not necessarily maximize the sum rate performance. However, this may happen in some cases as an extra benefit.

C. Average Sum Rate Performance

1) One-Tier Network: Fig. 13 demonstrates the average performance of the one-tier optical attocell network. First, the focus is on FR-VL and IB-VL backhaul systems. It is observed that general trends for both FR-VL and IB-VL systems are monotonically decreasing with respect to Φ_b. For FR-VL, the reason is that by widening the light beam, the backhaul interference on the downlink is increased and at the same time, the SINR of the backhaul links is reduced. For IB-VL, on the other hand, an increase in Φ_b causes the sub-band ratio δ to decrease because of the lower SINR of the backhaul links. This has suppressed the overall performance of the first tier since it is directly proportional to δ according to (21). Furthermore, it is observed that FR-VL outperforms IB-VL throughout the entire range of Φ_b regardless of the value of K_1, in spite of the fact that FR-VL causes a higher interference. This is achieved as a result of a better utilization of the bandwidth. For $\Phi_b = 5°$, the performance of the FR-VL network reaches the upper limit of 806 Mbits/s offered by the UB network. This is attributed in part to a substantial reduction in the backhaul interference for small values of Φ_b, in line with Theorem 1.

Fig. 13 shows the performance of FR-VL and IR backhaul systems including power control. For FR-VL, by comparing the cases (a) and (b), it can be observed that the performance

is significantly improved when the backhaul power is reduced by a factor of 10. The improvement is up to 188 Mbits/s for moderate values of Φ_b. This is primarily because by reducing the backhaul power, the adverse effect of backhaul interference is alleviated. In comparison to the case (b), the FR-VL case (c) that uses the optimal power ratio achieves a better performance until $\Phi_b = 25°$, at which $K_1^* = 0.1$. Note that $K_{1,\min} > 0.1$ for $\Phi_b > 25°$; see Fig. 5. In the case of IR, the bandwidth ratio is equal to one. Fig. 13 shows that IR backhauling performs near the UB limit especially for the cases (a) and (c) which correspond to $K_1 = 1$ and $K_1 = K_1^*$, for small to moderate values of Φ_b. This indicates that the power efficiency of the IR backhaul system can be remarkably improved by using the minimum power control coefficients given by (52), (53) and (54), depending on the value of Φ_b. This gain is attained while preserving the average sum rate performance identical to the case when using the full power for the IR backhaul system. In the IR case (b), where the power of the backhaul system is reduced by a factor of 100, no loss in performance is observed for $\Phi_b \leq 10°$, and the extent of performance loss is still sustainable for moderate to large values of Φ_b.

2) Two-Tier Network: Fig. 14 demonstrates the average sum rate performance of the two-tier optical attocell network. The UB network gives the constant upper limit of 1.91 Gbits/s for the network performance. In addition, the IB-VL network globally has the worst performance. Among the FR-VL cases, the case (c) using $K_1 = K_7 = K_8 = 0.1$ has the lowest performance. The other three cases take the same value of $K_1 = 1$. The low performance in the case (c) is due to a ten times reduction in the power of the bottleneck backhaul
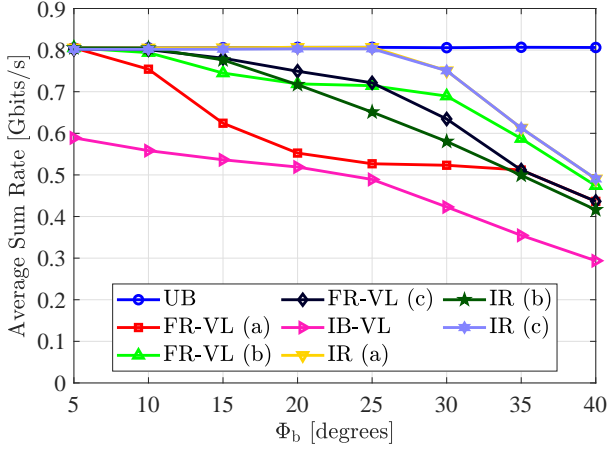
Fig. 13. Average sum rate performance of the one-tier optical attocell network using FR-VL, IB-VL and IR backhaul systems as a function of Φ_{b}. For FR-VL (a) $K_1 = 1$; (b) $K_1 = 0.1$; (c) $K_1 = K_1^*$. For IR (a) $K_1 = 1$; (b) $K_1 = 0.01$; and (c) $K_1 = K_1^*$. For IR backhaul, $B_{\mathrm{b}} = B_{\mathrm{a}}$.

Fig. 14. Average sum rate performance of the two-tier optical attocell network using FR-VL, IB-VL and IR backhaul systems as a function of Φ_{b}. For FR-VL case (a) $K_1 = K_7 = K_8 = 1$; (b) $K_1 = 1$, and $K_7 = K_8 = 0.1$; (c) $K_1 = K_7 = K_8 = 0.1$; and (d) $K_1 = 1$, and $(K_7, K_8) = (K_7^*, K_8^*)$. For IR case (a) $K_1 = K_7 = K_8 = 1$; (b) $K_1 = K_7 = K_8 = 0.01$; and (c) $K_j = K_j^*$ for $j = 1, 7, 8$. For IR backhaul, $B_{\mathrm{b}} = 3B_{\mathrm{a}}$.

link, which directly affects the sum rate performance of the network. The performance of the case (d) using the optimal power ratios of (K_7^*, K_8^*) is bounded from below by that of the case (a) and from above by that of the case (b), where (a) and (b) correspond to $K_7 = K_8 = 1$ and $K_7 = K_8 = 0.1$. The cases (a), (b) and (d) perform slightly better than the case (c). Furthermore, in the case of IR, a bandwidth ratio of three is used. It is evident that the performance of the case (c) using the minimized power ratios perfectly matches with the case (a) that uses the full power for the IR backhaul system, though using the minimum sum power. Likewise, the power of all the backhaul links can be reduced according to the value of Φ_{b} without degrading the network performance. This is achieved by choosing a sufficient bandwidth for the IR backhaul system, i.e., $B_{\mathrm{b}} = 3B_{\mathrm{a}}$.

VI. CONCLUSIONS

In this paper, a novel wireless backhaul solution is proposed for indoor optical attocell networks by which the BSs are connected to the gateway via multi-hop wireless optical links. For both FR-VL and IB-VL backhaul systems, the downlink performance depends upon the directivity of the light beam in the backhaul links. A better performance is achieved for a smaller value of Φ_{b}. In addition, FR-VL gives a significantly better performance than IB-VL, and it enables the network to attain the performance of a benchmark UB network particularly for a one-tier deployment. Following a power optimization for the backhaul system, the results suggest that FR-VL is not an appropriate option for network deployments of more than one tier. Alternatively, the migration of wireless optical backhauling to the IR band is proposed. In this case, after establishing a power-bandwidth tradeoff analysis for a two-tier network, IR backhauling shows the potential that it does not only outperform FR-VL backhauling but its performance is closely matched to that of the UB network in terms of the network sum rate, when using a properly designed divergence angle for the light beam in the backhaul links. For the IR backhaul system, given a modulation bandwidth of only three
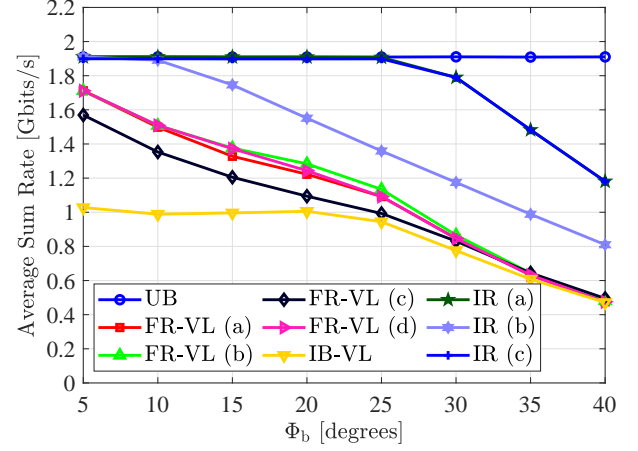
times that of the downlink VLC system, the backhaul transmission power can be made 100 times lower than the full power operation without influencing the network performance. This is a remarkable gain for power efficiency. Future directions include but are not limited to: 1) an investigation into the effect of imperfect alignment for an aimed wireless optical backhaul link on the overall network performance; 2) a study of the scaling laws of the presented power-bandwidth tradeoff for the design of wireless optical backhaul systems applied to multi-tier networks; and 3) an extension to other network deployment models.

APPENDIX A
PROOF OF THEOREM 1

The analysis is performed for the limit $\ell \to \infty$ which is equivalent to $\Phi_{\mathrm{b}} \to 0$. Based on (13) and (28), a unified expression is obtained for the backhaul interference effect as follows:

$$\mathcal{F}_{\mathrm{BI}}(z_u) = \frac{(\ell+1)^2}{(m+1)^2 h^{2m}} \sum_{j \in \mathcal{Q}_i} \frac{K_j r_s^{2\ell}(z_u) \cos^{2\ell}(\theta_s - \Theta_{\mathrm{b}_j})}{(r_s^2(z_u) + h^2)^{\ell+3}}. \tag{56}$$

Rearranging (56), and taking the limit $\ell \to \infty$, the asymptotic backhaul interference effect can be evaluated as:

$$\lim_{\ell \to \infty} \mathcal{F}_{\mathrm{BI}}(z_u) = \frac{1}{(m+1)^2 h^{2m}(r_s^2 + h^2)^3} \times$$
$$\lim_{\ell \to \infty} \sum_{j \in \mathcal{Q}_i} K_j(\ell+1)^2 \left[\frac{r_s^2 \cos^2(\theta_s - \Theta_{\mathrm{b}_j})}{r_s^2 + h^2} \right]^{\ell}. \tag{57}$$

In (57), the fraction inside the bracket is bounded as follows:

$$0 \leq \frac{r_s^2 \cos^2(\theta_s - \Theta_{\mathrm{b}_j})}{r_s^2 + h^2} < 1. \tag{58}$$

$$\frac{\partial \gamma_i^{\text{FR-VL}}}{\partial K_1} = -\frac{\mathcal{F}_1(z_i; \mathcal{Q}_i)\mathcal{S}(z_i)}{\left[K_1\mathcal{F}_1(z_i; \mathcal{Q}_i) + K_7\mathcal{F}_2(z_i; \mathcal{O}_i) + K_8\mathcal{F}_2(z_i; \mathcal{E}_i) + \mathcal{F}_{\text{ICI}}(z_i) + \Omega\right]^2} < 0, \tag{63}$$

Using (58), the limit of the two product terms that depend on ℓ under the summation in (57) can be calculated as:

$$\lim_{\ell \to \infty} (\ell+1)^2 \left[\frac{r_s^2\cos^2(\theta_s - \Theta_{\text{b}_j})}{r_s^2 + h^2}\right]^\ell = 0, \tag{59}$$

because, as $\ell \to \infty$, the term $[\ ]^\ell$ decays much faster than the term $(\ell+1)^2$ grows. Considering that K_j is a finite value under the summation in (57), substituting (59) into (57) yields:

$$\lim_{\ell \to \infty} \mathcal{F}_{\text{BI}}(z_u) = 0, \ \forall u, \tag{60}$$

hence the proof is complete.

APPENDIX B
MONOTONICITY OF $g_1(K_1, K_7, K_8)$ IN K_1

By taking the partial derivative of g_1 in (43) with respect to K_1, one can verify that:

$$\frac{\partial g_1}{\partial K_1} = \frac{\frac{\partial \gamma_{\text{b}_1}}{\partial K_1}}{1 + \gamma_{\text{b}_1}} - \sum_{i=1,7,8} \frac{\frac{\partial \gamma_i^{\text{FR-VL}}}{\partial K_1}}{1 + \gamma_i^{\text{FR-VL}}} > 0, \tag{61}$$

because:

$$\frac{\partial \gamma_{\text{b}_1}}{\partial K_1} = \frac{\left(\frac{1}{4}\right)^{\ell+1}K_7 + \frac{1}{\gamma_{\text{b}}}}{\left[2\left(\frac{1}{4}\right)^\ell K_1 + \left(\frac{1}{4}\right)^{\ell+1}K_7 + \frac{1}{\gamma_{\text{b}}}\right]^2} > 0, \tag{62}$$

and the partial derivative of $\gamma_i^{\text{FR-VL}}$ with respect to K_1 is always negative as shown in (63) at the top of the page. To derive (62) and (63), respectively, (25) and (9) are used.

APPENDIX C
A REMARK ON THE CONSTRAINT IN (44)

For sufficiently small values of Φ_{b}, according to Theorem 1, the backhaul interference effect tends to zero and $\mathcal{F}_{\text{BI}}(z_i) \approx 0$, $\forall i$, taking into account the last constraint of P2, $0 < K_j \le 1$ for $j = 1, 7, 8$. In such a case, $\gamma_i^{\text{FR-VL}}$ in (9) can be tightly approximated by $\gamma_i^{\text{FR-VL}} \approx \frac{\mathcal{S}(z_i)}{\mathcal{F}_{\text{ICI}}(z_i) + \Omega}$, which is independent of K_1, K_7 and K_8. In addition, provided that the optical power is concentrated within the backhaul links, the cross-coupling interference among them is insignificant. Thus, γ_{b_1} in (25) reduces to $\gamma_{\text{b}_1} \approx K_1\gamma_{\text{b}}$ and, by using (43), (44) simplifies to:

$$K_1 \ge \frac{\prod\limits_{i=1,7,8}\left(1 + \gamma_i^{\text{FR-VL}}\right) - 1}{\gamma_{\text{b}}} \ge \frac{\prod\limits_{i=1,7,8}\gamma_i^{\text{FR-VL}}}{\gamma_{\text{b}}}. \tag{64}$$

The second inequality is due to $\gamma_i^{\text{FR-VL}} \gg 1$, which typically holds at the center of an attocell and the optimization is based on the downlink SINR at the center of attocells. The RHS of (64) is an asymptotic bound for $K_{1,\min}(K_7, K_8)$ in (44).

APPENDIX D
MINIMUM ELEMENT OF THE FEASIBLE SET FOR P3

Let $K_7 = K_{7,\min}(K_8)$ and $K_8 = K_{8,\min}(K_7)$ be replaced by $x = g(y)$ and $y = f(x)$, respectively, and let (x_0, y_0) be their intersection point, to simplify notation. The feasible set can be expressed as:

$$\mathcal{D} = \left\{(x, y) \in \mathbb{R}_+^2 \big| x \ge g(y), y \ge f(x)\right\}. \tag{65}$$

As a geometric description, to say that (x_0, y_0) is the minimum element of $\mathcal{D}$ means that all other points of $\mathcal{D}$ lie to the right and above the point (x_0, y_0). More precisely, the objective is to prove that $(x_0, y_0) \preceq (x, y)$, $\forall(x, y) \in \mathcal{D}$, where $\preceq$ is induced by the positive quadrant $\mathbb{R}_+^2$ [39]. To this end, since f and g in (65) are increasing with respect to their arguments, by jointly expanding the conditions $x \ge g(y)$ and $y \ge f(x)$, one arrives at:

$$\begin{cases} x \ge g(y) \ge g(y_0) = x_0, \\ y \ge f(x) \ge f(x_0) = y_0, \end{cases} \tag{66}$$
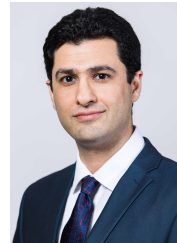
which is what was to be shown.

ACKNOWLEDGMENT

REFERENCES

[1] M. Figueiredo, L. N. Alves, and C. Ribeiro, "Lighting the Wireless World: The Promise and Challenges of Visible Light Communication," *IEEE Consum. Electron. Mag.*, vol. 6, no. 4, pp. 28–37, Oct. 2017.

[2] "Cisco Visual Networking Index: Global Mobile Data Traffic Forecast Update, 2016–2021," Cisco White Paper, Feb. 2017.

[3] H. Burchardt, N. Serafimovski, D. Tsonev, S. Videv, and H. Haas, "VLC: Beyond Point-to-Point Communication," *IEEE Commun. Mag.*, vol. 52, no. 7, pp. 98–105, Jul. 2014.

[4] H. Haas, L. Yin, Y. Wang, and C. Chen, "What is LiFi?" *IEEE/OSA J. Lightw. Technol.*, vol. 34, no. 6, pp. 1533–1544, Mar. 2016.

[5] C. X. Wang, F. Haider, X. Gao, X. H. You, Y. Yang, D. Yuan, H. M. Aggoune, H. Haas, S. Fletcher, and E. Hepsaydir, "Cellular Architecture and Key Technologies for 5G Wireless Communication Networks," *IEEE Commun. Mag.*, vol. 52, no. 2, pp. 122–130, Feb. 2014.

[6] V. Chandrasekhar, J. G. Andrews, and A. Gatherer, "Femtocell Networks: A Survey," *IEEE Commun. Mag.*, vol. 46, no. 9, pp. 59–67, Sep. 2008.

[7] C. Chen, D. A. Basnayaka, and H. Haas, "Downlink Performance of Optical Attocell Networks," *IEEE/OSA J. Lightw. Technol.*, vol. 34, no. 1, pp. 137–156, Jan. 2016.

[8] I. Stefan, H. Burchardt, and H. Haas, "Area Spectral Efficiency Performance Comparison between VLC and RF Femtocell Networks," pp. 3825–3829, Jun. 2013.

[9] D. J. F. Barros, S. K. Wilson, and J. M. Kahn, "Comparison of Orthogonal Frequency-Division Multiplexing and Pulse-Amplitude Modulation in Indoor Optical Wireless Links," *IEEE Trans. Commun.*, vol. 60, no. 1, pp. 153–163, Jan. 2012.

[10] D. Tsonev, S. Videv, and H. Haas, "Unlocking Spectral Efficiency in Intensity Modulation and Direct Detection Systems," *IEEE J. Sel. Areas Commun.*, vol. 33, no. 9, pp. 1758–1770, Sep. 2015.

[11] C. Chen, S. Videv, D. Tsonev, and H. Haas, "Fractional Frequency Reuse in DCO-OFDM-Based Optical Attocell Networks," *IEEE/OSA J. Lightw. Technol.*, vol. 33, no. 19, pp. 3986–4000, Oct. 2015.

[12] S. Chia, M. Gasparroni, and P. Brick, "The Next Challenge for Cellular Networks: Backhaul," *IEEE Microw. Mag.*, vol. 10, no. 5, pp. 54–66, Aug. 2009.

[13] K. Chandra, R. V. Prasad, and I. Niemegeers, "An Architectural Framework for 5G Indoor Communications," in *Proc. Int. Wireless Commun. Mobile Comput. Conf. (IWCMC)*, Aug. 2015, pp. 1144–1149.

[14] X. Li, F. Jin, R. Zhang, J. Wang, Z. Xu, and L. Hanzo, "Users First: User-Centric Cluster Formation for Interference-Mitigation in Visible-Light Networks," *IEEE Trans. Wireless Commun.*, vol. 15, no. 1, pp. 39–53, Jan. 2016.

[15] Z. Huang and Y. Ji, "Efficient user access and lamp selection in LED-based visible light communication network," *Chin. Opt. Lett.*, vol. 10, no. 5, p. 050602, May 2012.

[16] H. Ma, L. Lampe, and S. Hranilovic, "Coordinated Broadcasting for Multiuser Indoor Visible Light Communication Systems," *IEEE Trans. Commun.*, vol. 63, no. 9, 2015.

[17] T. Komine and M. Nakagawa, "Integrated System of White LED Visible-Light Communication and Power-Line Communication," *IEEE Trans. Consum. Electron.*, vol. 49, no. 1, pp. 71–79, Feb. 2003.

[18] J. Song, W. Ding, F. Yang, H. Yang, B. Yu, and H. Zhang, "An Indoor Broadband Broadcasting System Based on PLC and VLC," *IEEE Trans. Broadcast.*, vol. 61, no. 2, pp. 299–308, Jun. 2015.

[19] H. Ma, L. Lampe, and S. Hranilovic, "Hybrid Visible Light and Power Line Communication for Indoor Multiuser Downlink," *IEEE/OSA J. Opt. Commun. Netw.*, vol. 9, no. 8, pp. 635–647, Aug. 2017.

[20] P. Mark, "Ethernet over Light," Master's thesis, University of British Columbia, Dec. 2014.

[21] F. Delgado, I. Quintana, J. Rufo, J. A. Rabadan, C. Quintana, and R. Perez-Jimenez, "Design and Implementation of an Ethernet-VLC Interface for Broadcast Transmissions," *IEEE Commun. Lett.*, vol. 14, no. 12, pp. 1089–1091, Dec. 2010.

[22] Y. Wang, N. Chi, Y. Wang, L. Tao, and J. Shi, "Network Architecture of a High-Speed Visible Light Communication Local Area Network," *IEEE Photon. Technol. Lett.*, vol. 27, no. 2, pp. 197–200, Jan. 2015.

[23] C. W. Chow, C. H. Yeh, Y. Liu, C. W. Hsu, and J. Y. Sung, "Network Architecture of Bidirectional Visible Light Communication and Passive Optical Network," *IEEE Photon. J.*, vol. 8, no. 3, pp. 1–7, Jun. 2016.

[24] H. Kazemi, M. Safari, and H. Haas, "A Wireless Backhaul Solution Using Visible Light Communication for Indoor Li-Fi Attocell Networks," in *Proc. IEEE Int. Conf. Commun. (ICC)*, May 2017, pp. 1–7.

[25] H. Kazemi and H. Haas, "Downlink Cooperation with Fractional Frequency Reuse in DCO-OFDMA Optical Attocell Networks," in *Proc. IEEE Int. Conf. Commun. (ICC)*, May 2016.

[26] H. Kazemi, M. Safari, and H. Haas, "Spectral Efficient Cooperative Downlink Transmission Schemes for DCO-OFDM-Based Optical Attocell Networks," in *Proc. IEEE 84th Veh. Technol. Conf. (VTC Fall)*, Sep. 2016.

[27] J. M. Kahn and J. R. Barry, "Wireless Infrared Communications," *Proc. IEEE*, vol. 85, no. 2, pp. 265–298, Feb. 1997.

[28] S. Shao, A. Khreishah, M. Ayyash, M. B. Rahaim, H. Elgala, V. Jungnickel, D. Schulz, T. D. C. Little, J. Hilt, and R. Freund, "Design and Analysis of a Visible-Light-Communication Enhanced WiFi System," *IEEE/OSA J. Opt. Commun. Netw.*, vol. 7, no. 10, pp. 960–973, Oct. 2015.

[29] D. Tsonev, H. Chun, S. Rajbhandari, J. J. D. McKendry, S. Videv, E. Gu, M. Haji, S. Watson, A. E. Kelly, G. Faulkner, M. D. Dawson, H. Haas, and D. O'Brien, "A 3-Gb/s Single-LED OFDM-Based Wireless VLC Link Using a Gallium Nitride μLED," *IEEE Photon. Technol. Lett.*, vol. 26, no. 7, pp. 637–640, Apr. 2014.

[30] *Light and Lighting – Lighting of Work Places. Part I: Indoor Work Places*. British Standards Institution, BS EN 12464-1:2011.

[31] J. N. Laneman, D. N. C. Tse, and G. W. Wornell, "Cooperative Diversity in Wireless Networks: Efficient Protocols and Outage Behavior," *IEEE Trans. Inf. Theory*, vol. 50, no. 12, pp. 3062–3080, Dec. 2004.

[32] O. Narmanlioglu, R. C. Kizilirmak, F. Miramirkhani, and M. Uysal, "Cooperative Visible Light Communications With Full-Duplex Relaying," *IEEE Photon. J.*, vol. 9, no. 3, pp. 1–11, Jun. 2017.

[33] C. H. Chen, M. Hargis, J. M. Woodall, M. R. Melloch, J. S. Reynolds, E. Yablonovitch, and W. Wang, "GHz bandwidth GaAs light-emitting diodes," *Appl. Phys. Lett.*, vol. 74, no. 21, pp. 3140–3142, May 1999.

[34] E. F. Schubert, *Light-Emitting Diodes*, 2nd ed. Cambridge University Press, 2006.

[35] S. Dimitrov, S. Sinanovic, and H. Haas, "Clipping Noise in OFDM-Based Optical Wireless Communication Systems," *IEEE Trans. Commun.*, vol. 60, no. 4, pp. 1072–1081, Apr. 2012.

[36] O. Oyman and S. Sandhu, "A Shannon-Theoretic Perspective on Fading Multihop Networks," in *Proc. 40th Annual Conf. Inf. Sci. Sys. (CISS)*, Mar. 2006, pp. 525–530.

[37] S. Lu, V. Bharghavan, and R. Srikant, "Fair Scheduling in Wireless Packet Networks," *IEEE/ACM Trans. Netw.*, vol. 7, no. 4, pp. 473–489, Aug. 1999.

[38] T. Cover and A. E. Gamal, "Capacity Theorems for the Relay Channel," *IEEE Trans. Inf. Theory*, vol. 25, no. 5, pp. 572–584, Sep. 1979.

[39] S. Boyd and L. Vandenberghe, *Convex Optimization*. Cambridge University Press, Mar. 2004.

Hossein Kazemi (S'16) received the M.Sc. degree in Electrical Engineering, with a specialty in microelectronic circuits, from the Sharif University of Technology, Tehran, Iran, in 2011, and the M.Sc. degree (Hons.) in Electrical Engineering, with a focus in communication systems, from Özyeğin University, Istanbul, Turkey, in 2014. He is currently pursuing the Ph.D. degree in Electrical Engineering at the Institute for Digital Communications, University of Edinburgh, Edinburgh, U.K. His main research interests include wireless optical communications and networks.

Majid Safari (S08-M11) received his Ph.D. degree in Electrical and Computer Engineering from the University of Waterloo, Canada in 2011. He also received his B.Sc. degree in Electrical and Computer Engineering from the University of Tehran, Iran, in 2003, M.Sc. degree in Electrical Engineering from Sharif University of Technology, Iran, in 2005. He is currently an assistant professor in the Institute for Digital Communications at the University of Edinburgh. Before joining Edinburgh in 2013, he held postdoctoral fellowship at McMaster University, Canada. Dr. Safari is currently an associate editor of IEEE Communication letters. His main research interest is the application of information theory and signal processing in optical communications including fiber-optic communication, free-space optical communication, visible light communication, and quantum communication.

Harald Haas (S'98-AM'00-M'03-SM'16-F'17) received the Ph.D. degree from the University of Edinburgh in 2001. He currently holds the Chair of Mobile Communications at the University of Edinburgh, and is the Initiator, Co-Founder, and the Chief Scientific Officer of pureLiFi Ltd., and the Director of the LiFi Research and Development Center, the University of Edinburgh. He has authored 400 conference and journal papers, including a paper in Science and co-authored the book *Principles of LED Light Communications Towards Networked LiFi* (Cambridge University Press, 2015). His main research interests are in optical wireless communications, hybrid optical wireless and RF communications, spatial modulation, and interference coordination in wireless networks. He first introduced and coined spatial modulation and LiFi. LiFi was listed among the 50 best inventions in *TIME* Magazine 2011. He was an invited speaker at TED Global 2011, and his talk on "Wireless Data from Every Light Bulb" has been watched online over 2.4 million times. He gave a second TED Global lecture in 2015 on the use of solar cells as LiFi data detectors and energy harvesters. This has been viewed online over 1.8 million times. He was elected as a fellow of the Royal Society of Edinburgh in 2017. In 2012 and 2017, he was a recipient of the prestigious Established Career Fellowship from the Engineering and Physical Sciences Research Council (EPSRC) within Information and Communications Technology in the U.K. In 2014, he was selected by EPSRC as one of ten Recognising Inspirational Scientists and Engineers (RISE) Leaders in the U.K. He was a co-recipient of the EURASIP Best Paper Award for the *Journal on Wireless Communications and Networking* in 2015, and co-recipient of the Jack Neubauer Memorial Award of the IEEE Vehicular Technology Society. In 2016, he received the Outstanding Achievement Award from the International Solid State Lighting Alliance. He was a co-recipient of recent best paper awards at VTC-Fall, 2013, VTC-Spring 2015, ICC 2016, and ICC 2017. He is an Editor of the IEEE TRANSACTIONS ON COMMUNICATIONS and the IEEE JOURNAL OF LIGHTWAVE TECHNOLOGIES.